Annual Report on Contributions to ASRA-6C – A Commercial Stellarator Fusion Reactor

B. Badger, L.A. El-Guebaly, Gilbert A. Emmert, Gerald L. Kulcinski, Edwin M. Larsen, John F. Santarius, Mohamed E. Sawan, John E. Scharer, Igor N. Sviatoslavsky, William F. Vogelsang, Peter L. Walstrom and Layton J. Wittenberg

December 23,

FPA-85-4

FUSION POWER ASSOCIATES

2 Professional Drive, Suite 248
Gaithersburg, Maryland 20879
(301) 258-0545

1500 Engineering Drive
Madison, Wisconsin 53706
(608) 263-2308

ANNUAL REPORT ON CONTRIBUTIONS TO

ASRA-6C - A COMMERCIAL STELLARATOR FUSION REACTOR

by

B. Badger, L.A. El-Guebaly, Gilbert A. Emmert, Gerald L. Kulcinski, Edwin M. Larsen, John F. Santarius, Mohamed E. Sawan, John E. Scharer, Igor N. Sviatoslavsky, William F. Vogelsang, Peter L. Walstrom and Layton J. Wittenberg

December 23, 1985

FPA-85-4

I. INTRODUCTION

A joint study was initiated in 1985 between the Max Planck Institut für Plasmaphysik (IPP), Garching, FRG; the Kernforschungszentrum (KfK), Karlsruhe, FRG; and Fusion Power Associates (FPA), Madison, WI. This scoping study was aimed at identifying the key critical issues associated with the design of a 1 GWe fusion power plant based on the stellarator concept.

The study was divided between the three groups as follows:

IPP - Plasma Physics and Vacuum Magnetic Field Calculation
KfK - Magnet Design and Reactor Maintenance
FPA - Impurity Control, Blanket and Shield Design.

In the course of this year's work, several other issues were raised and incorporated into the work performed by each group. It was also discovered that a certain degree of overlap between the groups was desirable. Therefore some work on the magnets was performed by FPA, some work on blankets was performed by KfK, and some work on impurity control was performed by IPP.

Two major meetings were held during the year at which the three groups compared progress, integrated their findings, and planned for future work; the first meeting was held at Schloss Ringberg in the FRG on July 8 and 9, 1985. The second meeting was held in Madison, Wisconsin, USA on November 11 and 12, 1985. From the FPA side, the major contributions to the Schloss Ringberg meeting were the demonstration that the blanket and shield could be greatly reduced in thickness, thus allowing a much more efficient magnet set to be designed, and several proposals for pumped limiter designs. One of the major contributions from FPA to the second meeting in Madison was a poloidal and toroidal analysis of the neutron wall loading which dictated the design requirements for shielding of magnets. A more detailed analysis on the magnetic "island" design for a pumped limiter after the Ringberg meeting was

somewhat negative and it was agreed at the Madison meeting to investigate other possibilities. In addition, work was also presented on a fundamental approach to magnet winding considerations for the complex ASRA coils.

The purpose of this brief report is to restate the highlights of our findings over the past year. It does not contain all of the details of the calculations performed (those were presented at the two meetings previously mentioned) nor does it review the concepts which were investigated but dropped after they appeared less promising.

The overall conclusions of this year's activities are included at the end of this report along with recommendations for future work.

II. IMPURITY CONTROL

The work on impurity control for ASRA-6C has focused on two issues: 1) the feasibility of using a pumped limiter to intercept the plasma diffusing out of the region of good magnetic surfaces, and 2) the use of ICRF to induce impurity flow reversal and thereby remove impurities from the hot, confined plasma.

II.1 Pumped Limiter Analysis

The primary problem with pumped limiters in tokamaks is that ions hitting the front face, or "crown," of the limiter blade recycle back into the plasma as neutral atoms. This produces an intense, localized flux of energetic charge exchange neutrals which impinge on the front face of the limiter and nearby areas of the first wall and erode them by sputtering. The function of the crown is to spread the incident power over a large area to reduce the power density to a manageable level and reduce the heat flux at the "limiter tip." This occurs because the shape of the crown places the limiter tip deeper in the scrape-off zone where the heat flux is lower. Magnetic divertors don't have this problem since the magnetic topology shifts the peak heat flux from the tip to the target plate in the collector chamber, where radiation, charge exchange cooling, and geometrical effects significantly spread the power deposition profile.

We have been investigating the use of the magnetic geometry of the stellarator to accomplish the same effect in ASRA-6C. The basic idea is to use a chain of magnetic islands to determine the boundary of the region of good magnetic surfaces. The present ASRA-6C magnetic configuration exhibits a chain of 11 islands at the plasma edge. This configuration is not ideal, but represents a starting point for the analysis of this concept. The pumped limiter

structure (blade, target plate, etc.) is placed inside an island, as shown schematically in Fig. II.1-1. One expects the particle and energy flux of the plasma escaping from the confinement region to peak on the island separatrix. This protects the limiter tip, which is placed deep inside an island. Furthermore, little plasma is incident on the front face and hence the generation of cold atoms reentering the hot plasma and the subsequent generation of energetic charge-exchange neutrals hitting the limiter crown and first wall is greatly reduced. The dominant interaction of the plasma with material surfaces is inside the limiter chamber where the plasma temperature is low and the neutrals are prevented by the structure and the incoming plasma from reaching the hot plasma. In addition, a high neutral pressure is produced there; this alleviates the problems with vacuum pumping.

This rather ideal view of a pumped limiter protected by a magnetic island is based on the assumption that the ions in the scrape-off zone follow the magnetic field lines in and near the islands. In addition to the motion along $\vec{B}$, the ions can drift across $\vec{B}$ because of field gradients and possible electric fields. Ions can also become trapped in magnetic wells and thereby be prevented from following the field lines. Ion-ion collisions cause pitch-angle scattering and lead to detrapping of ions trapped in magnetic wells. In addition, one is concerned about the "connection length" in the scrape-off zone. By this we mean the distance the average ion has to travel along $\vec{B}$ to reach the pumped limiter. If this is too long, the effectiveness of the pumped limiter is compromised.

We have made a preliminary estimate of the magnitude of these effects for ASRA-6C to see if they could defeat this concept. Neglecting electric field effects, we estimate the connection length to be of the order of 10^4 meters,

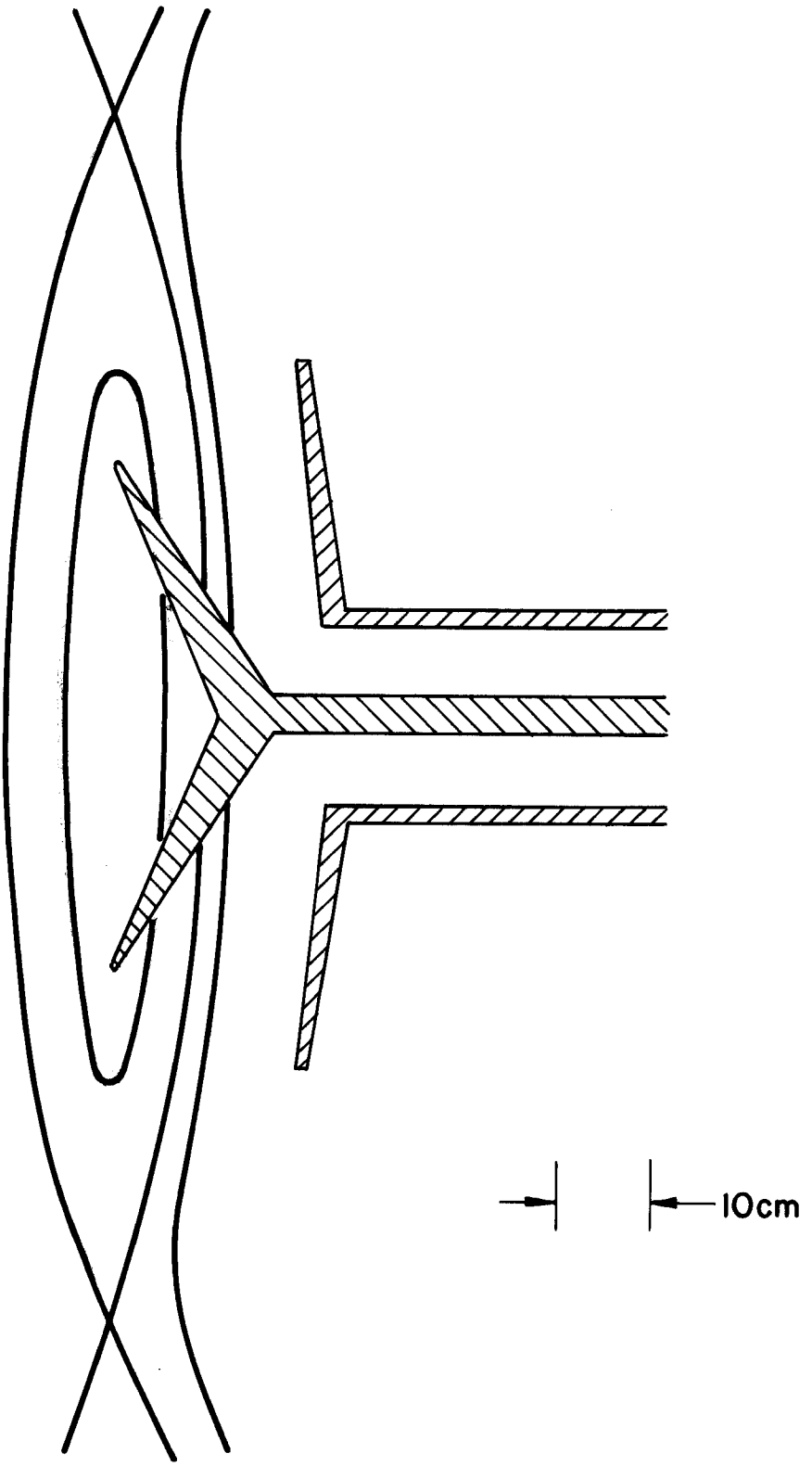

Fig. II.1-1 Magnetic island -- pumped limiter.

which corresponds to about 80 toroidal transits, using the magnetic island structure in ASRA-6C. To estimate guiding-center drift and collisional effects, we assumed the plasma temperature was 100 eV and the density was 10^{12} cm^{-3} in the scrape-off zone. These values are representative of edge values in tokamak modeling and are reasonable estimates for ASRA-6C, assuming parallel transport to the pumped limiter is the dominant loss process. The distance an ion drifts (due to magnetic curvature) in one toroidal transit is only 0.4 cm for these parameters; hence in one toroidal transit a circulating ion follows the field lines closely. In eighty transits, however, an ion could drift as much as 25 cm, if the drift were always in the same sense away from the magnetic surface. The islands are typically about 25-50 cm wide, so a 25 cm drift could be a concern. Fortunately, the drift is sometimes out of the island and sometimes into the island. This occurs because of the changing direction of $\vec{\nabla}B$ as the island winds around the torus. It is difficult to estimate the net drift after many toroidal transits, but it should be much less than 25 cm and therefore small compared with the island width.

The alternating direction of the grad-B drift does not occur for ions trapped in magnetic wells. The magnetic mirror ratio in the islands is typically about 1.2. Consequently, about 40% of the ions are trapped in magnetic wells. The collision frequency, however, of the plasma in the scrape-off zone is sufficiently high (at 100 eV and 10^{12} cm^{-3}) such that the typical ion mean free path is about 130 m (one toroidal transit). Hence an ion can only drift of the order of 0.3-0.4 cm before its pitch angle has scattered enough for the ion to become a circulating ion.

The presence of an electric field can also affect the ion motion through the $\vec{E} \times \vec{B}$ drift. The electric drift is in the magnetic surface if we assume

the magnetic surfaces are also equipotential surfaces. This appears reasonable because of the high electron mobility along the field lines. If we assume the potential is of the order of kT_e and varies on the scale of the island half-width, then the electric drift (100 m/s) increases the rate of precession of an ion around the island such that it now requires only about 11 toroidal transits to reach the pumped limiter. Electric drift effects cause the magnetic island-pumped limiter concept to work better.

The above considerations have to do with single particle and collective plasma effects influencing the ability of an ion to reach the target plate of a pumped limiter. They assume an ideal magnetic geometry of the island chain. On this basis the idea looks promising and merits further investigation. Magnetic islands, however, are due to subtle resonances between magnetic field perturbations and the background magnetic field. Calculations done for ASRA-6C at Garching indicate that, while these island structures can be found in calculations, they are very sensitive to errors (misaligned coils, slight shifts in the currents, currents in the plasma, etc.) and consequently, may be difficult to realize in a controlled and predictable way in practice. Consequently, the collective decision at the last joint meeting with KfK and IPP-Garching was to set aside the magnetic island-pumped limiter concept for now and pursue an alternative concept for particle and energy removal. This concept is to bound the plasma with a region where the magnetic field is ergodic and the plasma can be cooled by radiation and charge exchange. If this region is dense enough, then the interior hot plasma is shielded from neutral atoms and an energetic charge exchange flux is not generated. This approach is currently under investigation.

II.2 Impurity Control and Heating for ASRA-6C Utilizing ICRF

We have made a preliminary examination of methods for moderate to high Z active impurity control and heating to ignition utilizing ion cyclotron range of frequencies (ICRF) heating. The subjects examined include the use of localized ICRF heating which produces an azimuthal E_θ field which can reverse the flux-averaged radial flow for impurities in collisional and banana regimes. An estimate shows that about 11 MW of power could be considered to produce the necessary impurity flow reversal for the 1 GWe ASRA-6C stellarator reactor. We also suggest that this method for heating to ignition together with pellet injection for refueling is worth considering for the ASRA-6C reactor.

The potential steady-state operation of advanced stellarator reactor designs such as ASRA-6C means that considerable attention to impurity and heat removal must be made to allow it to operate in an optimum manner which allows full realization of its potential as a fusion reactor. One can ask the question whether passive particle diffusion and heat flow utilizing a divertor are sufficient or whether an active method for impurity control is required. We have considered two methods utilizing localized ICRF heating to address the problem of active impurity control methods. First, Ohkawa[1] has proposed the use of poloidal ion density inhomogeneities caused by heating to produce a poloidal electric field which leads to an impurity ion distribution and flow reversal in circular or noncircular tokamaks. We have examined this concept for ASRA-6C where $\varepsilon_t \simeq \varepsilon_h$. A second method utilizing cyclotron resonant ICRF heating with the range of anticipated impurity ion cyclotron species resonance is suggested for an enhanced radial transport which can then be removed by divertor action.

We first consider the large aspect ratio limit for a classical tokamak in the collisional regime with an ICRF heating mechanism which produces a poloidal asymmetry in the majority deuterium ion distribution. The helical ripple in ASRA-6C should be about 5% at r/a = 0.6 which is less than or comparable to the toroidal inverse aspect ratio of about 7%. The heated deuterium ion distribution is assumed to have a poloidal distribution given by $n_D = n_D(r)\ (1 + \cos\theta)$ where θ is the usual poloidal angle. This can be readily produced by heated banana trapped ion distributions which have been measured in minority ion heating experiments on PLT and computed in bounce averaged reactor heating computations by Harvey et al.[2] Figure II.2-1 illustrates this situation. The resulting poloidal electric field and poloidal variation in the impurity ion distribution can be average over a flux surface[1] to yield the net radial flux for species Z as

$$\Gamma_Z = (2\pi) \int r\, R n_Z V_{Zr} d\theta$$

$$= - \frac{(2\pi)^2 Ze(m_i/m_e)^{1/2} R B_\phi^2 n_i n_Z}{B_\theta^2 B^2} \times \left(- \frac{1}{en_i} \frac{\partial p_i}{\partial r} + \frac{1}{Zen_Z} \frac{\partial p_Z}{\partial r}\right)\left(3\varepsilon^2 - \frac{Z\varepsilon n_b}{(1 + Z_{eff})n_e}\right) .$$

Thus the radial flux is reversed when

$$\frac{n_b}{n_e} > \frac{3\varepsilon_t(1 + Z_{eff})}{Z}$$

and is most effective on high Z impurities.

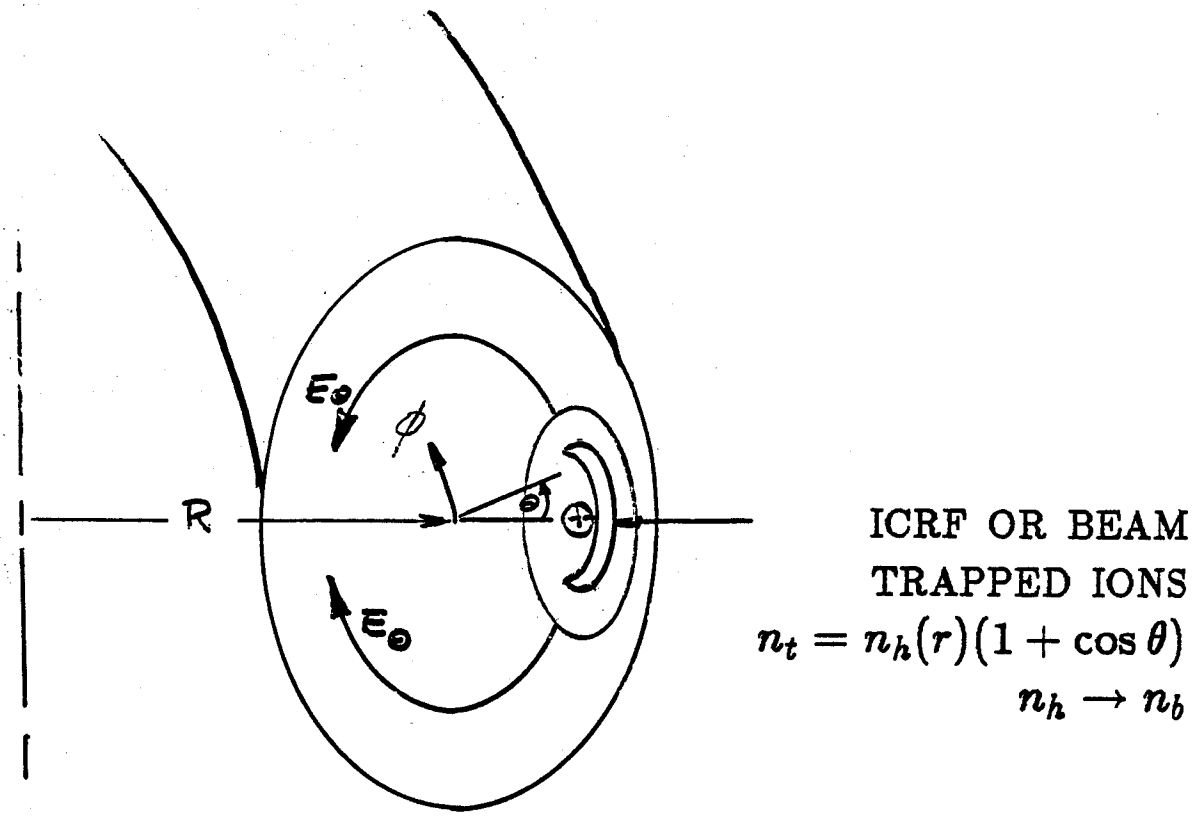

Fig. II.2-1. Diagram of heated charge distribution for impurity flow reversal.

Let ASRA-6C parameters be $Z_{eff} = 2$, $\varepsilon_t = 1.6/20 = 0.08$, and $Z_{Fe} = 26$. Impurity outflux criteria yields

$$n_b/n_e > 2\% \ .$$

Thus one may be able to heat a localized region where power requirements are in the range of $P_h \simeq 10$ MW to cleanse the plasma and improve fusion output.

We also note that Harvey et al.[2] have calculated the maximum poloidal ion density variation for a tokamak reactor as shown in Fig. II.2-2. Scaling this result for ASRA-6C we find that at r/a = 0.6 that an absorbed power density of $p = 0.5$ W/cm^3 with a density of 5×10^{13}/cm^3 at 8 keV with a localized absorption area of 1/50 of the poloidal cross section yields a poloidal ion density variation of 3-5% required for flow reversal. This yields an ICRF power source of $P = 0.5$ W/cm^3 x 1760 cm^2 x 2π x 2000 cm = 11 MW which is a small fraction of the supply needed for ignition and of the 1 GWe power output of the reactor. A 130 cm by 30 cm waveguide launcher of 2 m radial depth can be considered to couple 10 MW of ICRF power fed by a 30 cm diameter coaxial feed as shown in Fig. II.2-3.

We have also begun to consider the details of the ICRF heating in the stellarator as started by Kovrizhnykh et al.[3] We find that fundamental majority heating absorption for ASRA-6C should be an order of magnitude over that for a comparable tokamak due to the multiple resonant zones in the helical ripple and larger fraction of the flux surface over which the resonance occurs. Corresponding improvements are anticipated at higher harmonics which are currently being examined.

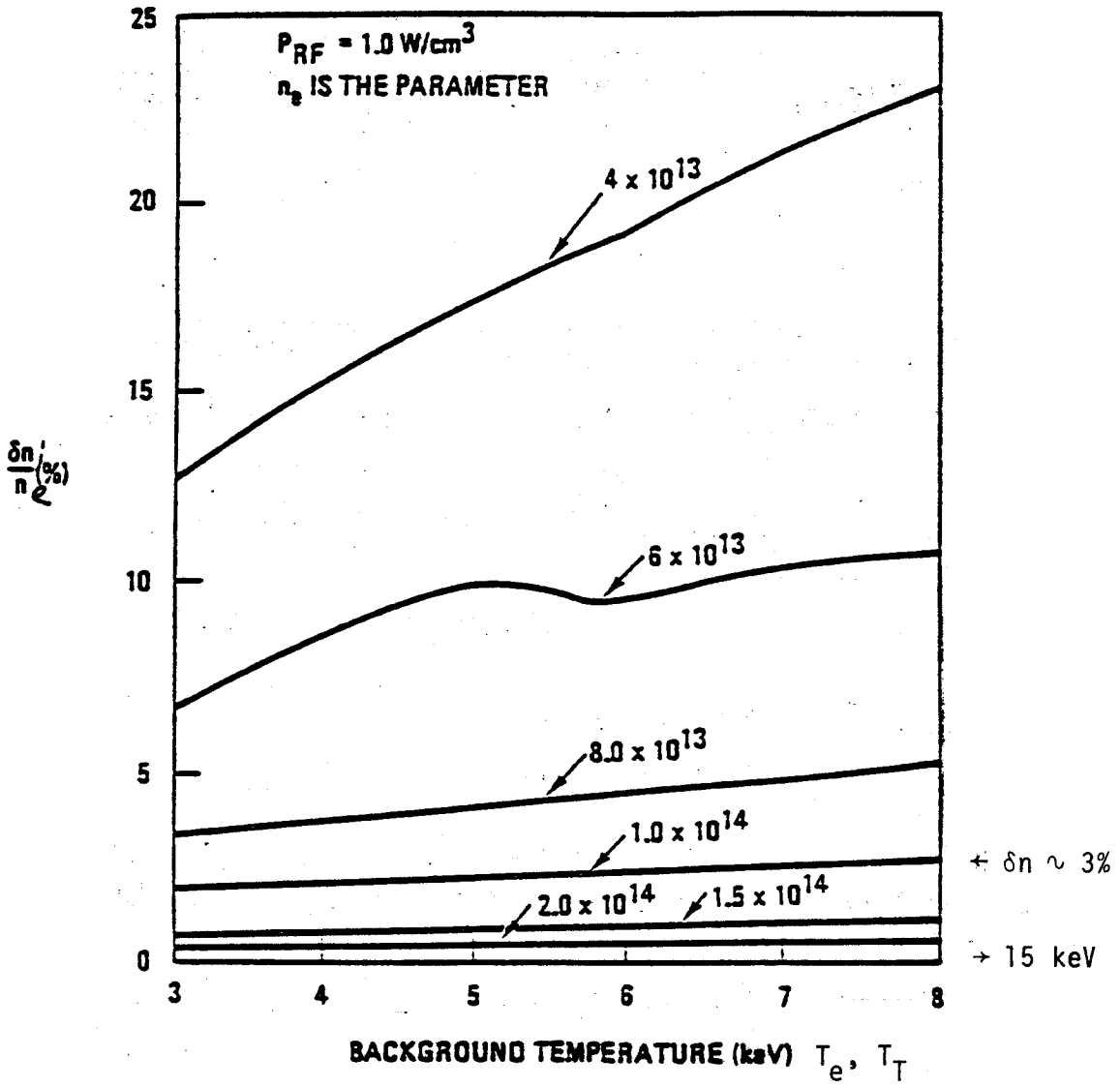

Fig. II.2-2. Maximum poloidal ion density variation versus background temperature. Electron density is a parameter and the absorbed rf power is 1 W/cm^3.

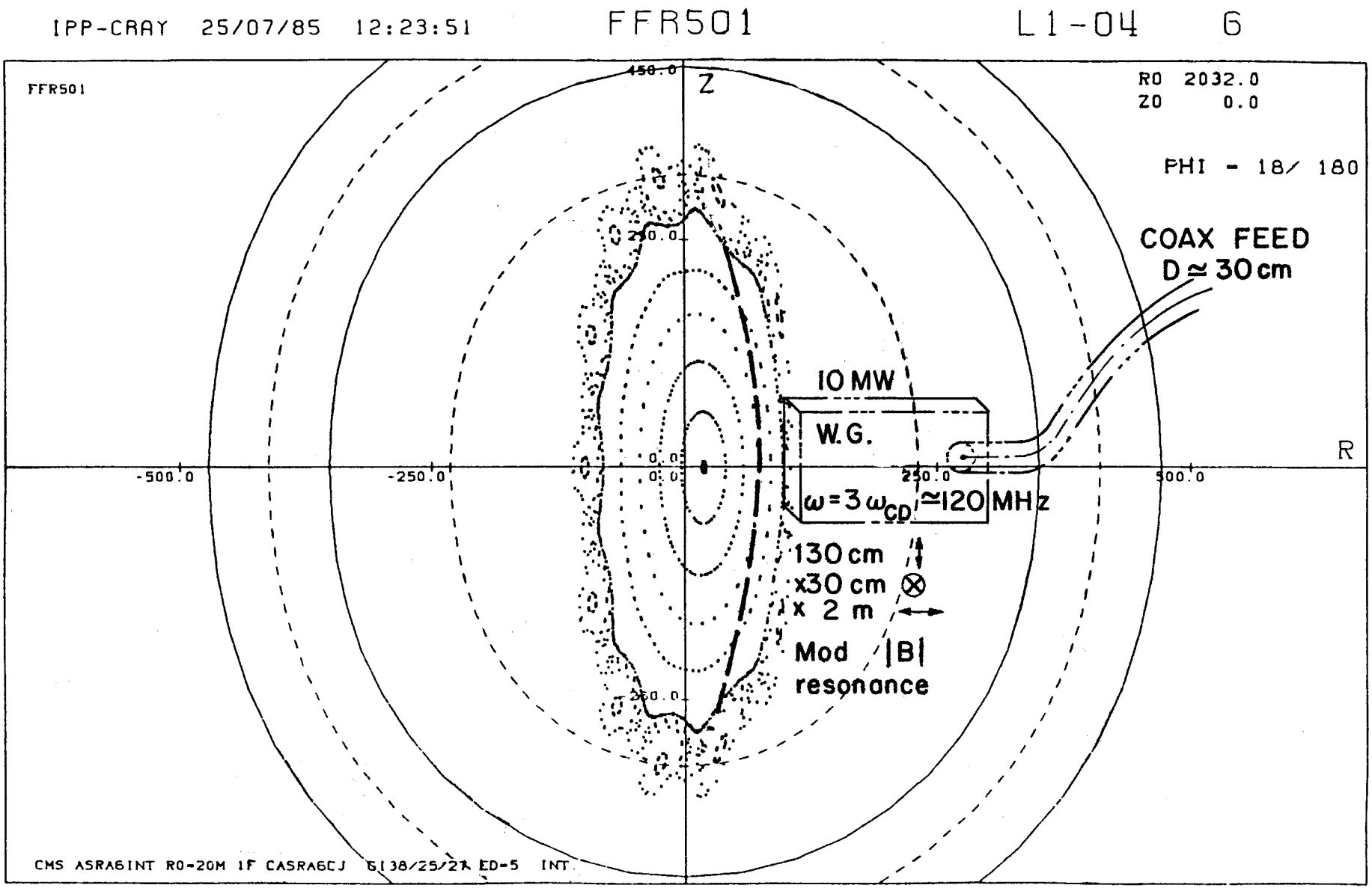

Fig. II.2-3. 10 MW ICRF Waveguide Launcher Configuration

We also note that argon impurity influx experiments on TFR and PLT have shown that ICRF heating can retard and reduce the concentration at the center when compared to the case without ICRF heating. In addition, isotope separation processes are used to spin up minority ion concentrations of a particular Z/A to the plasma edge for collection as are currently being carried out at TRW. Perhaps these techniques can be applied for active impurity control.

References

1. T. Ohkawa, "Prevention of Impurity Accumulation in Classical Tokamaks," GA Technologies Report GA-A17719, published in Kakuyugo-Kenkyo (1985).

2. R. Harvey et al., "ICRF Heating Fusion Reactivity Enhancement," to appear in Nuclear Fusion (1986).

3. L. Kovrizhnykh and P. Moroz, "Enhancement of Cyclotron Absorption of a Fast Magnetosonic Wave in Stellarators," IAEA-CN-44-F-IV-7, p. 633-642, Vol. 1, Proc. 10th Conf. on Plasma Physics & Controlled Nuclear Fusion Research (London), IAEA, 1985.

III. BLANKET

III.1 Design

The proposed blanket for the ASRA-6C stellarator power reactor is a He-gas-cooled design utilizing $Li_{17}Pb_{83}$ breeding material, HT-9 ferritic stainless steel structure and Be as a moderator/multiplier.

Over the years, there have been many He-gas-cooled blankets proposed for fusion reactor application. In most of these designs, the high pressure He gas was contained within the external blanket structure, making it effectively a pressure vessel, and the breeding material was contained in small tubes. We have reversed the order of containment in the proposed blanket, namely the high pressure gas is kept in small tubes which are immersed in a close packed matrix of Be balls and the remaining spaces filled with $Li_{17}Pb_{83}$ breeding material. The result is a compact blanket of 18 cm nominal thickness, in which only the tubes are operated in a stressed condition. The blanket external structure, however, is designed to withstand the consequence of a He-gas leak in one or more coolant tubes.

One of the problems which blankets utilizing liquid metals have is that the maximum temperatures of the liquid metal/structural interface must be kept low enough to be consistent with prescribed corrosion guidelines. We have solved the problem in two ways. First, the blanket temperature is kept relatively low (< 550°C) by allowing the He gas to gain temperature in the reflector where there are no liquid metals. Thus, the He gas first passes through the blanket reaching an intermediate temperature and then is routed through the reflector, reaching a high enough temperature to give a very respectable power cycle conversion efficiency. Secondly, the liquid metal in the blanket is static and, therefore, corrosion product transport does not

exist. In this way we have eliminated one of the most limiting restrictions which liquid metal blanket designs have had to contend with.

The proposed blanket consists of a series of cells of 20 cm nominal width connected together to form a blanket module. Figure III.1-1 is a midplane cross section of a proposed blanket module of arbitrary toroidal extent. The toroidal extent of a module can be varied by adding or subtracting cells, and depends on such aspects as allowable header dimensions and maintenance considerations. The width of a cell varies poloidally to provide the needed toroidicity for the module.

The plasma envelope in ASRA-6C permits the use of an elliptical blanket of constant cross section along the toroidal direction. A vertical cross section is shown in Fig. III.1-2. This figure shows the module with six coolant headers which alternately supply and return the He-gas coolant. Each supply header feeds He gas in both directions, with the tubes terminating in return headers. Figure III.1-3, which is a partial circumferential cross section, shows this very clearly. It shows a supply header with coolant tubes running poloidally in both directions toward return headers. Figure III.1-4 is a cross section of a cell showing the coolant tubes immersed in the $Be/Li_{17}Pb_{83}$.

There are two types of tubes called outer and inner. The outer tubes cool the front and rear zones of the blanket including the first wall. On leaving the supply header, each outer tube makes only four loops inside the cell, then travels in the back of the cell the remaining distance to the return header. The next outer tube crosses over the four loops of the preceding tube, then executes four loops of its own before exiting to the return header. From the plasma side, it appears as if only one tube spirals

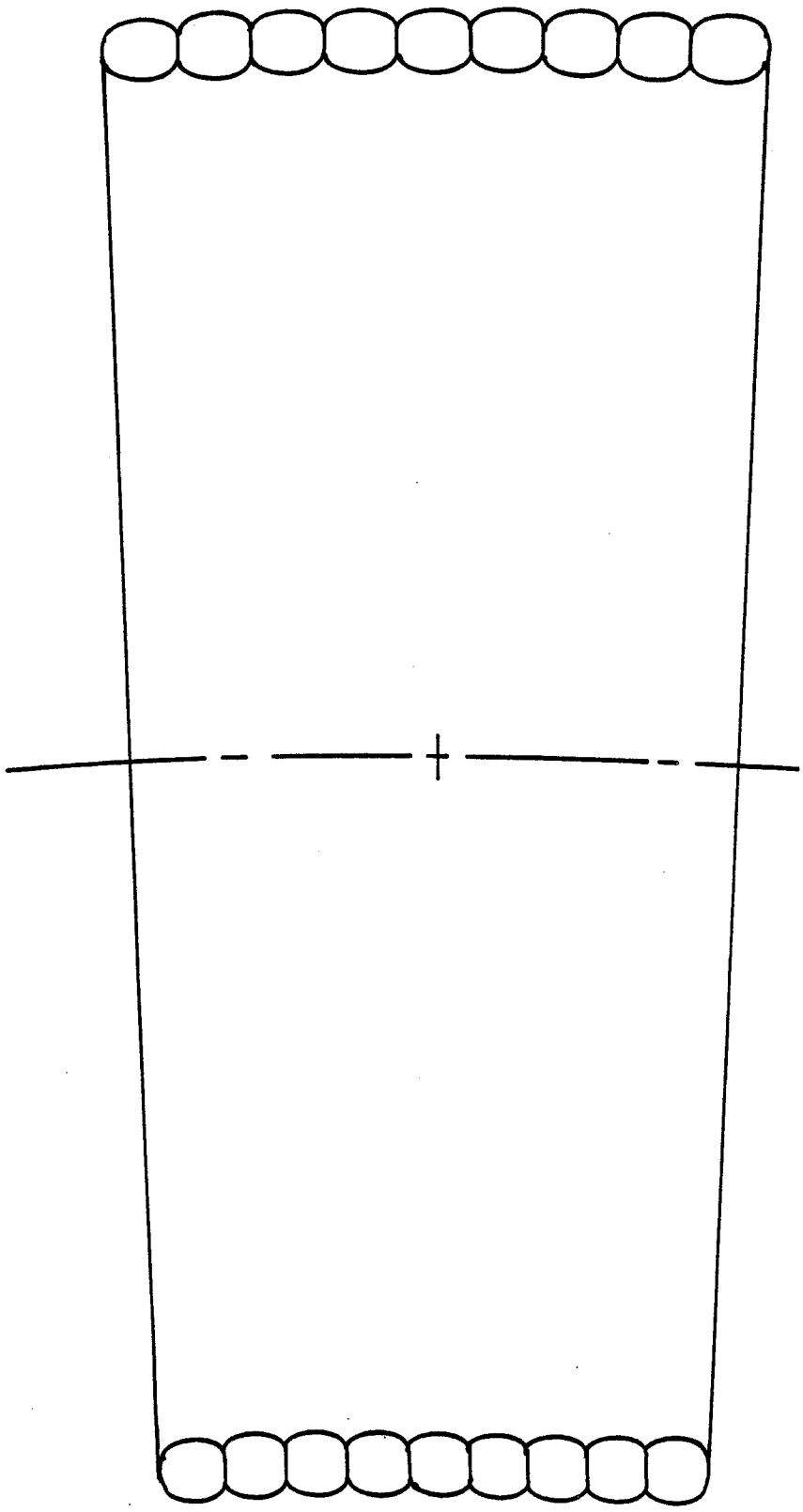

Fig. III.1-1. Midplane cross section of proposed blanket.

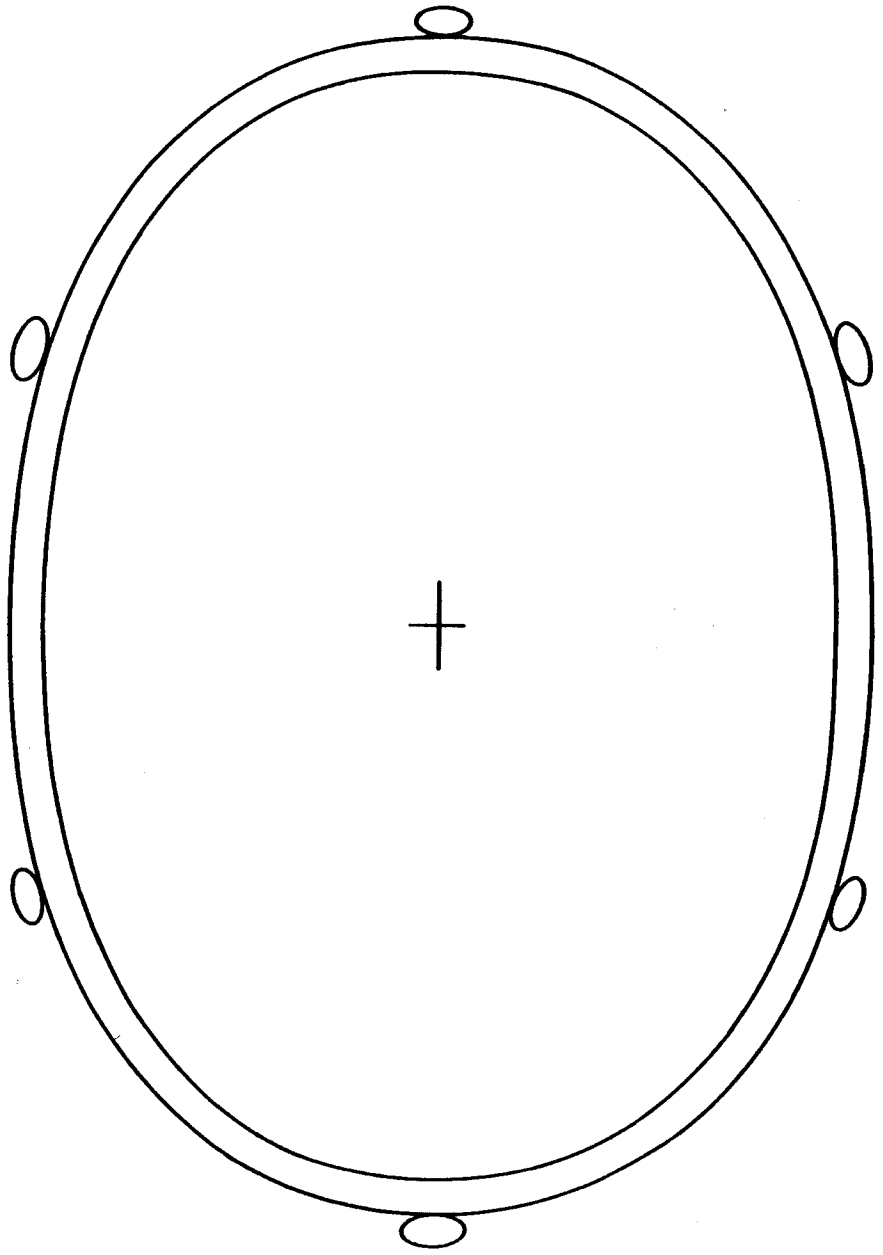

Fig. III.1-2. Vertical cross section of proposed blanket.

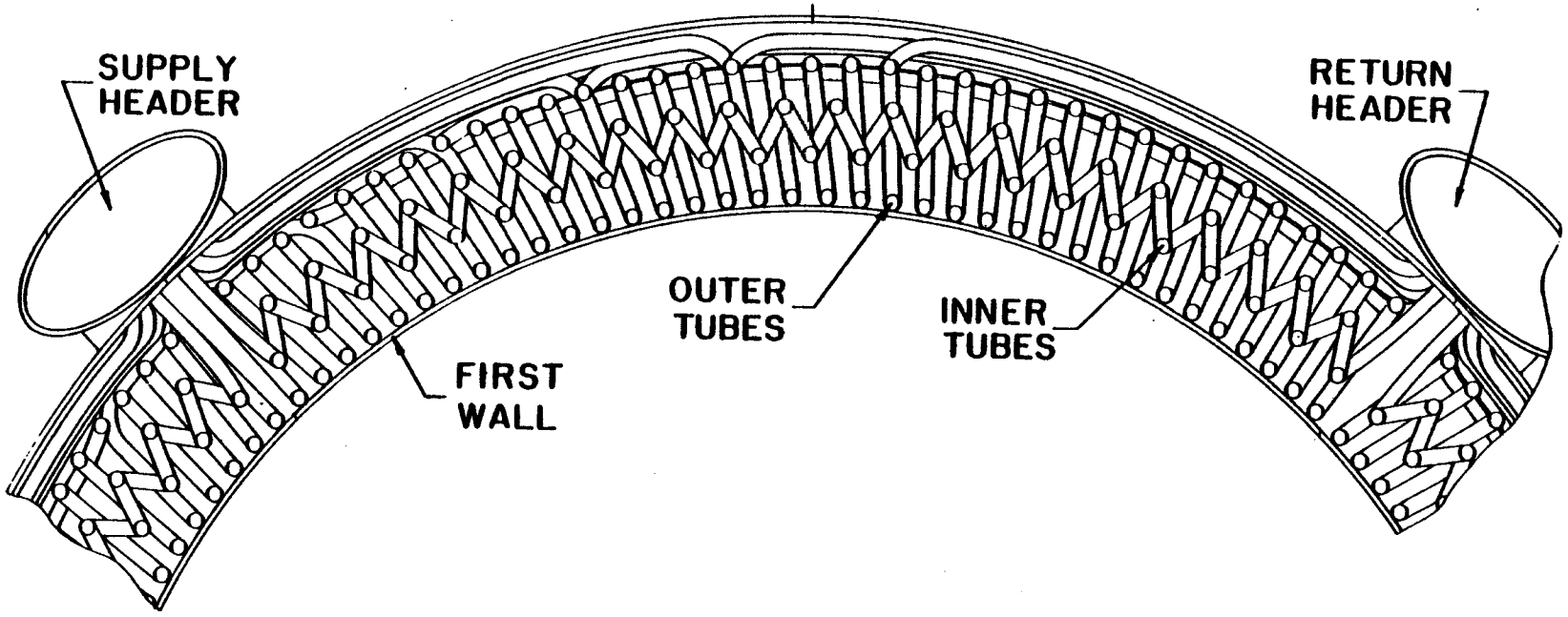

Fig. III.1-3. Partial vertical cross section of blanket showing coolant tubes.

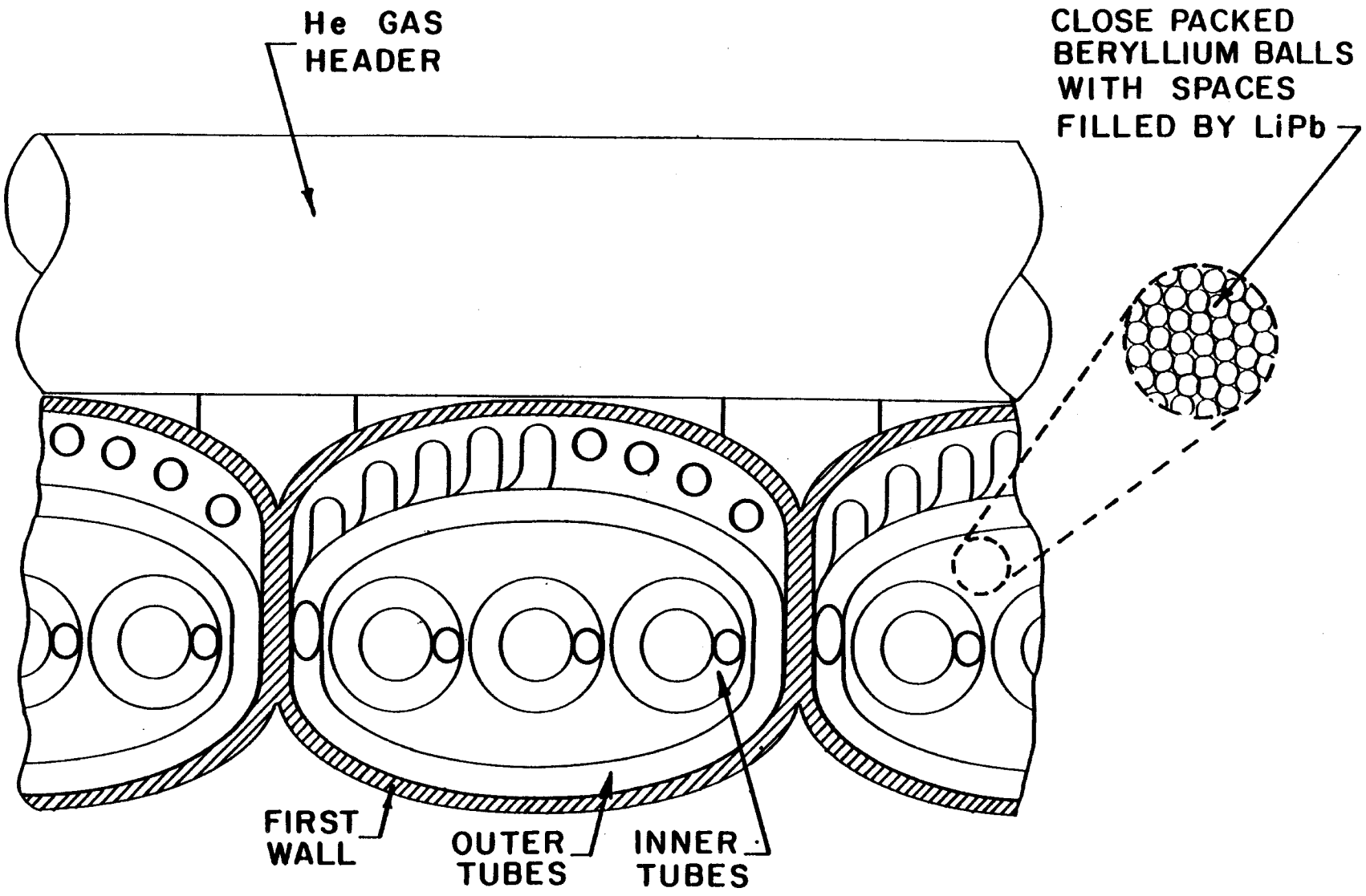

Fig. III.1-4. Cross-sectional view of several blanket cells.

around the circumference of the cell, but in fact there are many. The inner tubes, of which there are three, travel the full length between headers executing a large-pitch small-radius spiral. They provide a heat sink for nuclear heating in the center of the cell, and have the same length as the outer tubes. This design is unique because the length of all the tubes is the same, therefore, the pressure drop and mass flow rate are the same, insuring that none of the tubes will be starved for He gas flow.

The He gas pressure selected for this design is 80 atm. A trade study has shown that 80 atm seems to be the point at which the benefits of lower pumping power begin to be offset by the increased structure in the blanket.

The He gas enters the blanket at 275°C and exits at ~ 480°C, then is routed through the steel reflector exiting at the final temperature of 575°C before it goes on to the steam generator. A power cycle gross efficiency of 42.7% can be achieved with these conditions, assuming double reheat.

It is anticipated that the surface wall heating in ASRA-6C will be on the order of 20 W/cm^2 and the peak nuclear heating in the first wall is ~ 20 W/cm^3. An HT-9 first wall of 0.52 cm thickness will have a thermal stress of 60 MPa under these conditions.

The blanket also must be capable of accommodating penetrations such as pumpout ports and neutral beam ports. Penetrations which extend ~ 40 cm in the toroidal direction can be easily achieved in this type of design. Such penetrations occupy the space of two cells in which the tubes are shunted to the side as shown in Figs. III.1-5 and III.1-6. The poloidal extent of a penetration is only limited by the location of the headers and can be quite large. Penetrations larger than 40 cm characteristic toroidal dimension can be accommodated with some major local modifications of the blanket design.

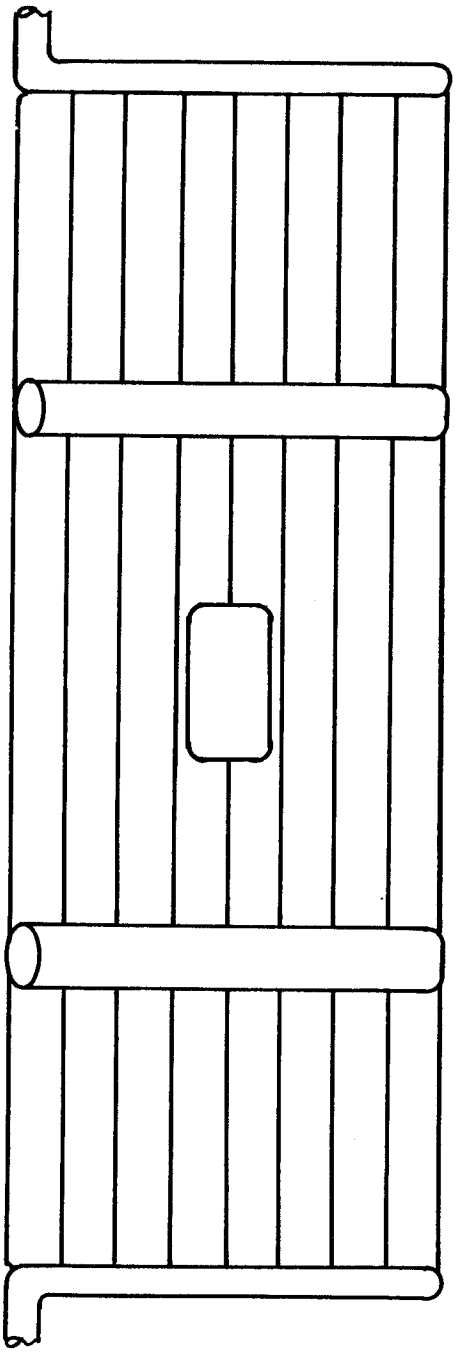

Fig. III.1-5. Rear view of blanket module showing a penetration.

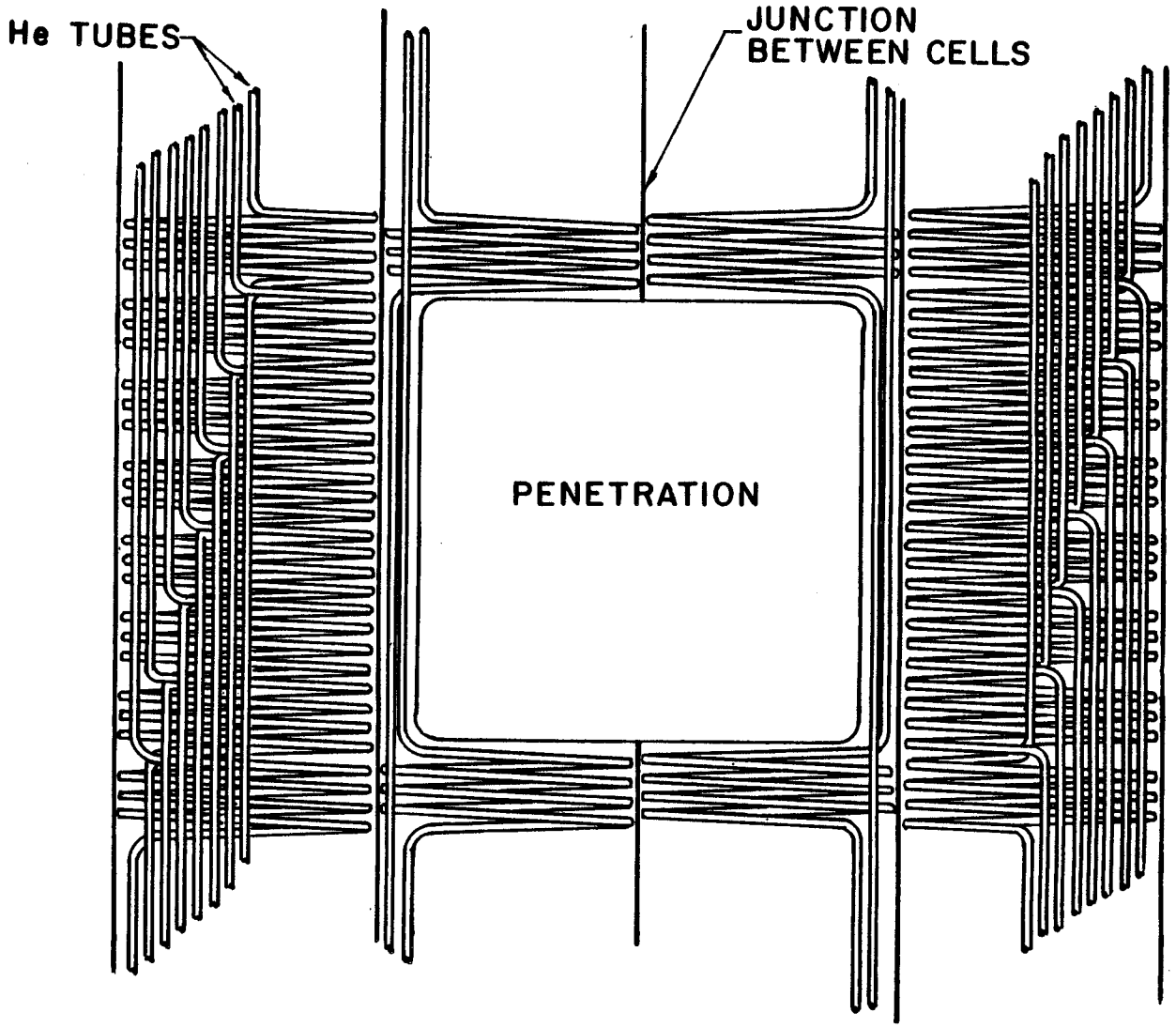

Fig. III.1-6. Typical penetration showing tube routing.

In summary, the proposed blanket has many attractive features with respect to high efficiency, economics and safety, and seems to be well suited for adoption in the ASRA-6C stellarator power reactor.

III.2 Blanket Neutronics

The main function of a fusion reactor blanket is to breed tritium and convert the fusion neutron kinetic energy into heat. In addition, providing adequate magnet protection is a major goal of the blanket and shield design. Since breeding blankets are not effective shields, a reduction in magnet size and overall reactor cost can be achieved by designing thin breeding blankets with more effective shielding materials used to protect the magnets.

$Li_{17}Pb_{83}$ is an attractive choice for the breeding material where the breeder and multiplier are intermixed. Due to the soft spectrum in such systems using highly enriched lithium (90% ^6Li) is beneficial. Almost all tritium breeding in this system results from the $^6Li(n,\alpha)t$ reaction which has a 1/V cross section. This implies that further enhancement in the tritium breeding ratio (TBR) and consequently further blanket thinning can be accomplished by using a moderator in the blanket. Hydrogen and hydrogen compounds are the best candidates. Beryllium has the dual advantage of acting as a moderator and multiplier. A series of one-dimensional neutronics calculations has been performed using ONEDANT[1] and ENDF/B-V data to analyze the LiPb, LiPb/TiH_2, and LiPb/Be helium cooled blanket concepts. A 10% He fraction and 10% HT-9 fraction was used in the analysis. Adding 10% TiH_2 enhances the TBR by 30% but the energy multiplication (M) drops by 8%. On the other hand, using 70% Be increases the TBR by 66% and M by 18%. Figure III.2-1 compares the neutronics performance of the three blanket concepts. It is clear that for a given required TBR, the LiPb/Be concept yields the thinnest blanket with largest M. This concept was chosen for the ASRA-6C blanket.

Using LiPb/Be results in a breeding blanket thickness in the range of 15-20 cm. The optimum combination of breeder and Be that maximizes the TBR in

THE T–M PLOTS FOR THE DIFFERENT BLANKET DESIGNS
(BLANKET THICKNESS VARIED)

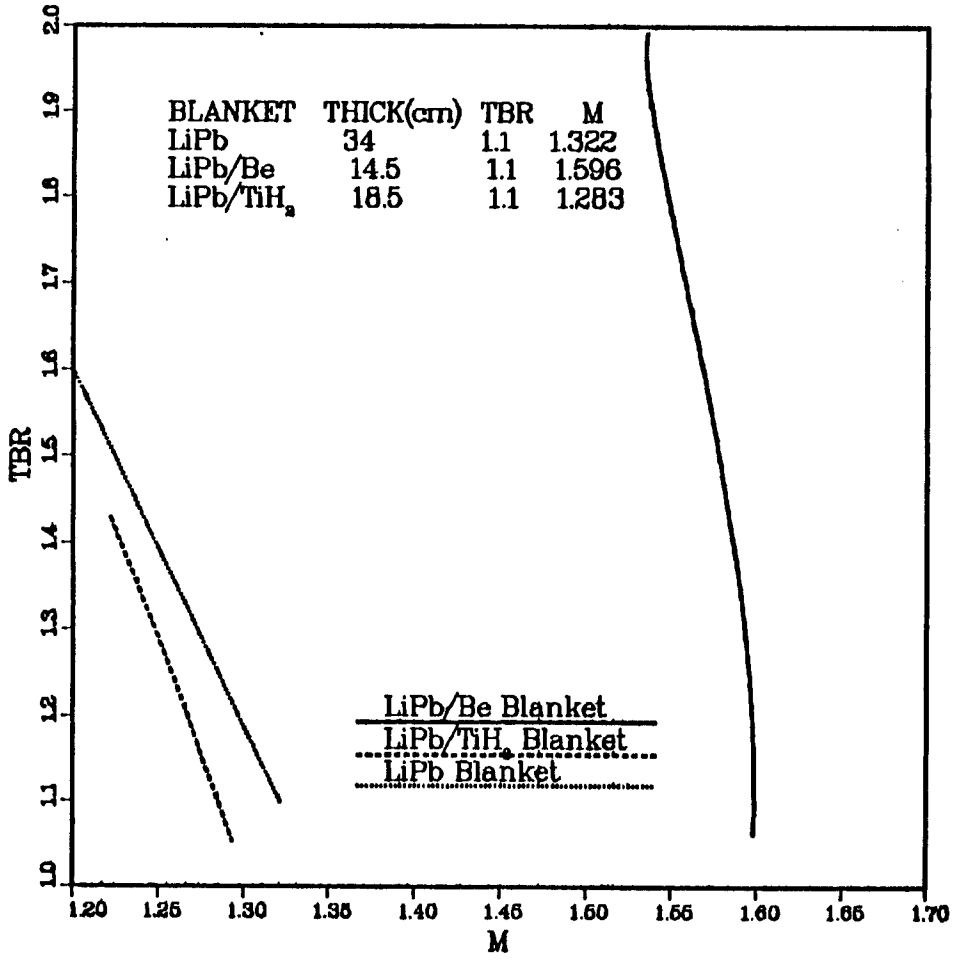

Fig. III.2-1. The tritium breeding-energy multiplication (T-M) plot for the different blanket concepts.

such a thin blanket was found to be 21% LiPb and 79% Be. Beryllium with 90% of the theoretical density is used to allow for swelling upon irradiation in the reactor. Due to the small Li inventory in the thin LiPb/Be blanket, the Li will be depleted rapidly and the TBR will decrease during operation. The effect of ^{6}Li depletion on the TBR is given in Fig. III.2-2. Frequent reprocessing is required to replace depleted Li. In the stationary LiPb blanket used for ASRA-6C, this can be done in a batch process. It is required that ASRA-6C achieve an overall TBR of 1.05. To achieve this time averaged overall TBR, the blanket must be designed with a higher initial TBR which is related to the time between LiPb replacement.

Many iterations were performed to determine the blanket thickness and the breeder, structure, and He content that satisfy all requirements for neutronics, thermal hydraulics, and mechanical design. The final blanket design consists of 14% $Li_{17}Pb_{83}$ (90% ^{6}Li), 52.57% Be (0.9 d.f.) and 11.03% HT-9 with the balance being void and He coolant. The blanket is 17.5 cm thick with a 1 cm thick first wall consisting of 50% HT-9 and 50% He gas. This yields an initial local TBR of 1.142. Only 0.05% of the TBR is contributed by the $^{7}Li(n,n'\alpha)t$ reaction. The penetrations required for pumping ducts, NBI ducts and ECRH ducts were estimated to occupy 3% of the 2190 m^2 first wall area in ASRA-6C. This implies an initial overall TBR of 1.108. To achieve an average overall TBR of 1.05, a 10% drop in TBR can be allowed before Li replenishment is needed. This corresponds to ~ 50% ^{6}Li depletion as indicated by Fig. III.2-2. LiPb replacement will be needed every 3.5 FPY's which does not impact the plant availability.

The breeding blanket is backed by a hot HT-9 reflector that consists of 90% HT-9 and 10% He. In addition to recovering the energy of neutrons and

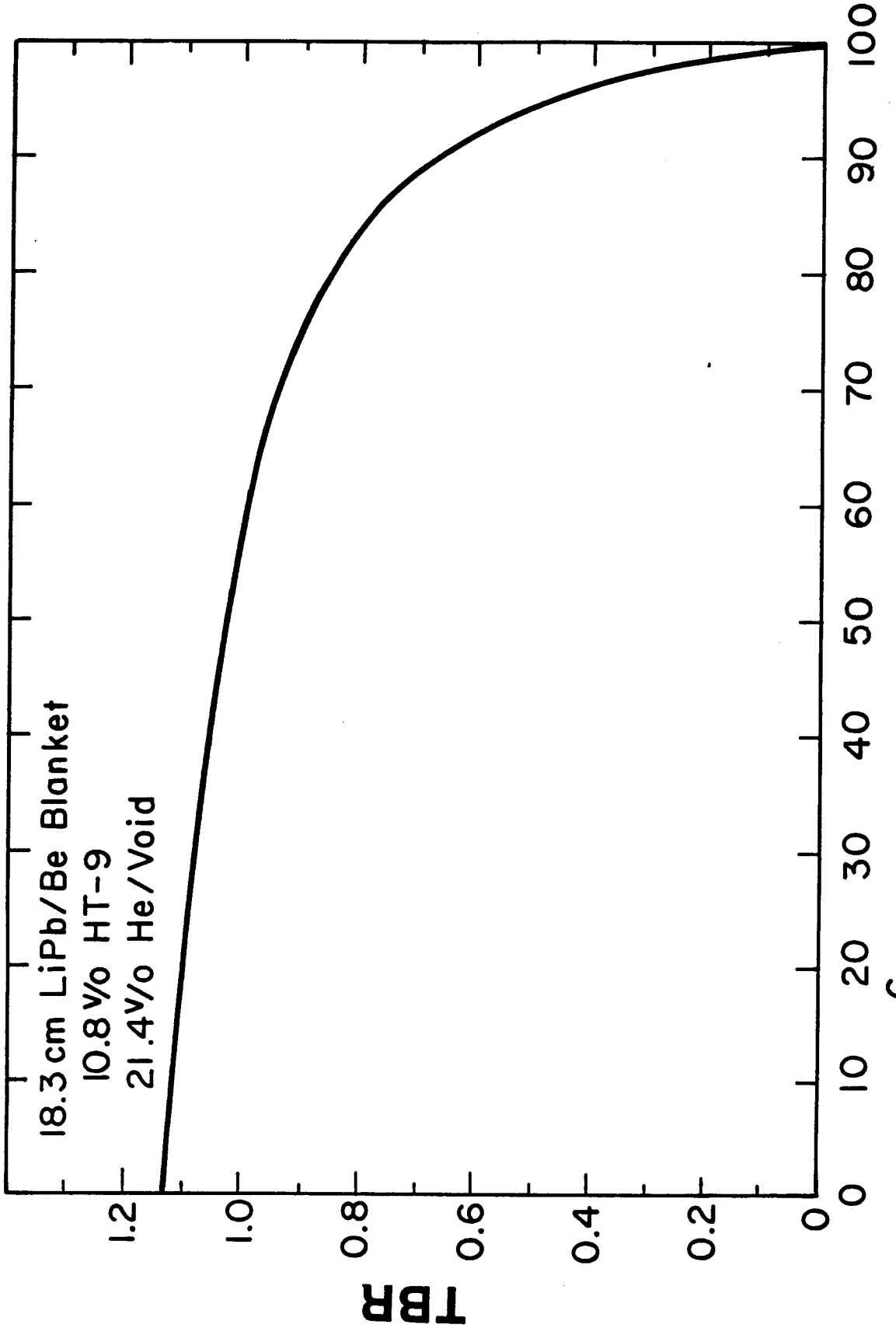

Fig. III.2-2. Effect of ^{6}Li depletion on TBR in the LiPb/Be/He blanket.

gammas leaking from the blanket, the reflector acts as the first layer of the magnet shield. The shield optimization, discussed in Section IV.2, indicates that the steel shield should occupy 58.1% of the shield thickness. The space available for the shield in ASRA-6C is 78.5 cm implying a reflector thickness of 45.6 cm. The corresponding value of the energy multiplication (M) is 1.42. Thirty-three percent of this energy is deposited in the reflector. About 48% of the nuclear heating is contributed by gamma heating. This M value corresponds to the initial local conditions. The reduction due to the penetrations is counterbalanced by the increase due to Li depletion yielding a time averaged overall energy multiplication which is nearly the same as the initial local M.

The neutron wall loading distribution in ASRA-6C was determined using the NEWLIT code.[2] The code assumes toroidal symmetry with a symmetric plasma shape about the reactor midplane. Two calculations were performed for the two toroidal locations where the plasma is horizontal (ϕ = 0°) and vertical (ϕ = 36°). The plasma outer boundary was fitted to a D-shape at each of the two toroidal locations. The magnetic shift was taken to be 50% of the plasma radius at the reactor midplane. The neutron source in the plasma was considered to vary with distance from the magnetic axis as $\{1-(a/a_p)^2\}^2$. The results were normalized to a reactor fusion power of 3.8 GW. The first wall has the same elliptic shape at all toroidal locations with a = 2.32 m and b = 3.23 m. The plasma parameters obtained by D-shape fitting at the toroidal locations d = 0° and 36° are given in Table III.2-1.

The results for the toroidal location ϕ = 0° are shown in Fig. III.2-3. The wall and plasma shapes are indicated as well as the source distribution. The results at ϕ = 36° are given in Fig. III.2-4. The results indicate that

Table III.2-1. Plasma Parameters at $\phi = 0°$ and $36°$ Obtained By Fitting the Boundary to $R = R_p + a_p \cos(t + C_p \sin t)$ and $Z = a_p \kappa_p \sin t$

	$\phi = 0°$	$\phi = 36°$
Plasma major radius R_p (m)	19.78	20.46
Plasma minor radius a_p (m)	2	0.93
Plasma elongation factor κ_p	0.765	3.07
Plasma triangularity factor C_p	0.52	0
Magnetic shift ε_m (m)	1	0.46

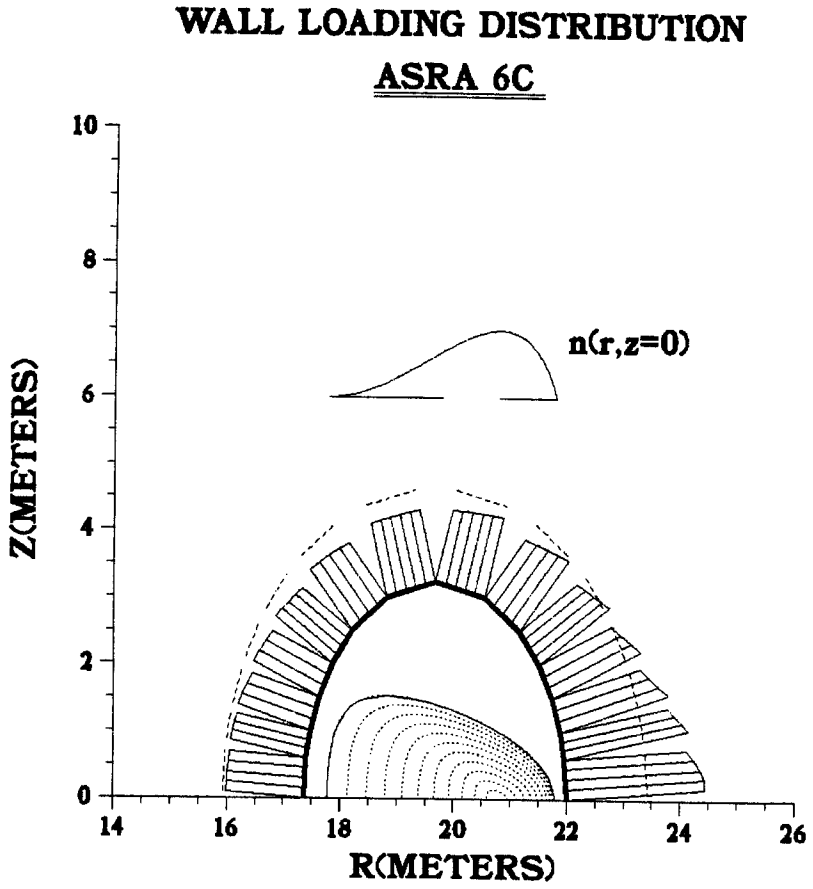

Fig. III.2-3. Neutron wall loading distribution at the toroidal location $\phi = 0°$.

Beginning of Field Period
ϕ=0°

Max Γ = 2.4 MW/m^2 at χ =0°

Min Γ = 1.1 MW/m^2 at χ =100°

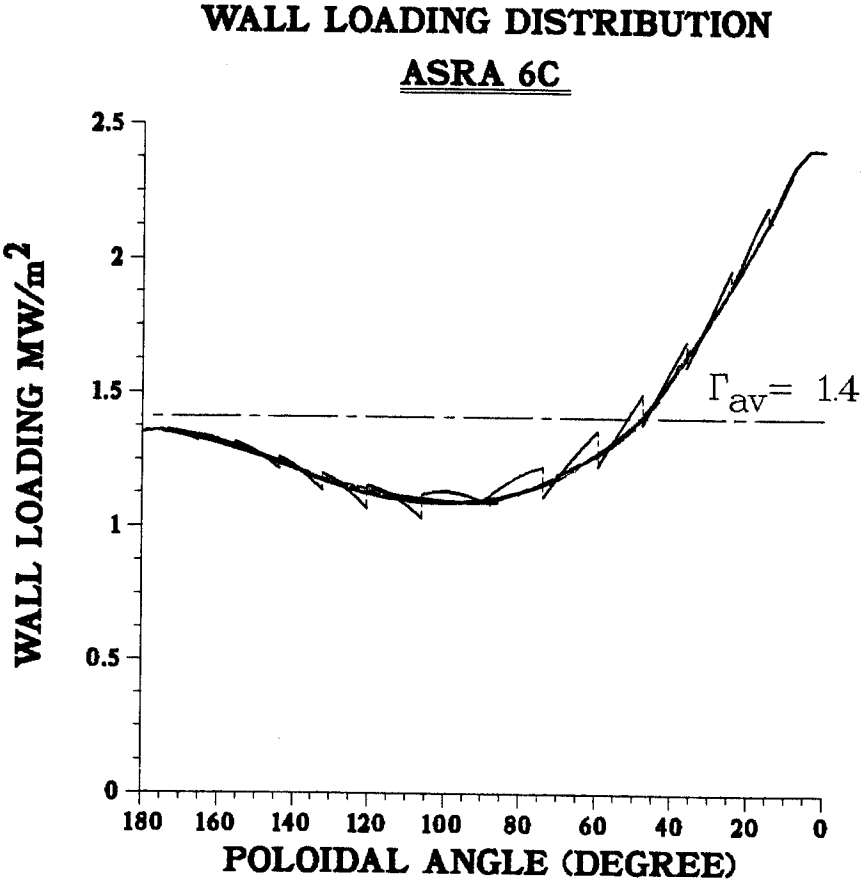

Figure III.2-3b.

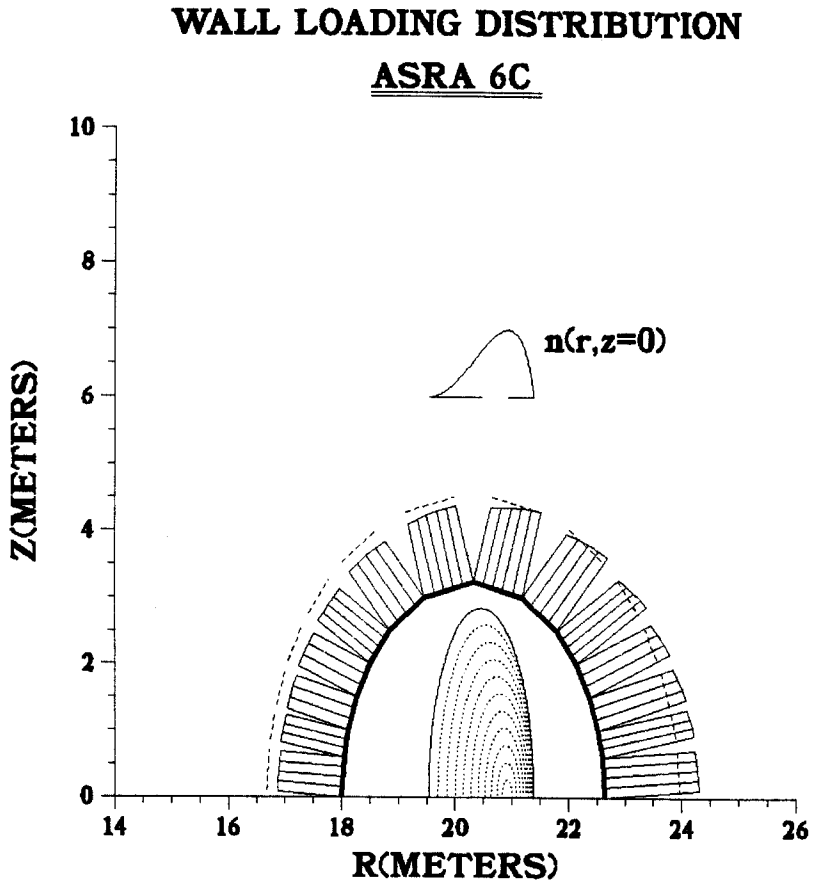

Fig. III.2-4. Neutron wall loading distribution at the toroidal location $\phi = 36°$.

Middle of Field Period
ϕ=36°

Max Γ = 1.7 MW/m^2 at χ =0°

Min Γ = 1.1 MW/m^2 at χ =120°

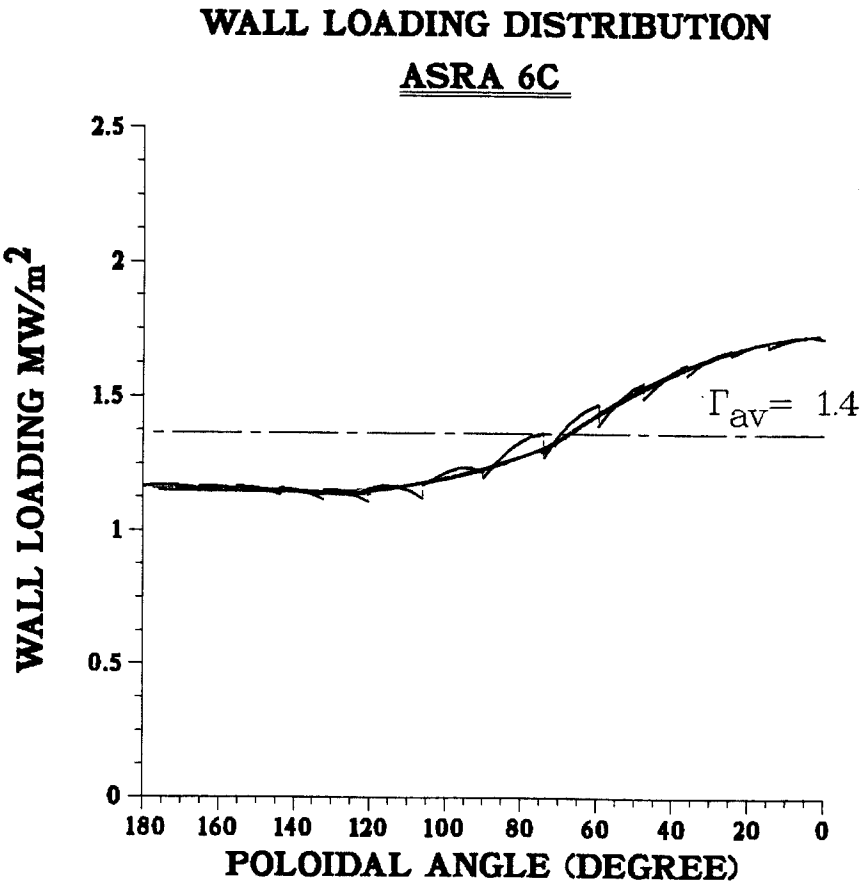

Fig. III.2-4b.

at all toroidal locations, the peak neutron wall loading occurs on the outboard side at the reactor midplane. The peak neutron wall loading in ASRA-6C is 2.4 MW/m^2 and occurs at the five toroidal locations where the plasma shape is horizontal. This peak value calculated by NEWLIT, which assumes axisymmetry, is a good estimate since the peak neutron source is nearly at the same distance from the major axis at all toroidal locations. The peak value is 70% higher than the average neutron wall loading of 1.4 MW/m^2.

References

1. R. O'Dell et al., "User's Manual for ONEDANT: A Code Package for One-Dimensional, Diffusion-Accelerated, Neutral Particle Transport," LA-9184-M, Los Alamos National Laboratory (1982).

2. H. Attaya and M. Sawan, "NEWLIT - A General Code for Neutron Wall Loading Distribution in Toroidal Reactors," Fusion Technology, 8/1, 608 (1985).

III.3 Tritium Removal from Breeder Blanket

The liquid breeder alloy, $Li_{17}Pb_{83}$, is being considered initially for the stellarator design in which the liquid alloy remains stationary in the breeder blanket, composed of the ferritic steel alloy HT-9. Tubes containing flowing helium are interspersed within the blanket to remove the heat and some of the tritium which is generated. The selection of this design has several advantages, namely: (1) the liquid metal is not pumped from the blanket for heat or tritium removal; therefore, the MHD pressure opposing the flowing liquid metal around the complex magnetic fields is not a factor, and (2) the liquid metal breeder releases the bred tritium in elemental form, T_2, while an oxide ceramic breeder predominantly releases tritium as T_2O; hence, T_2 can permeate the breeder tubes and be removed with the coolant while tritium oxide must be removed in a separate purge stream which adds complexity to the blanket design.

Although it is advantageous to transport the bred T_2 in the helium coolant, some technique must be used to lower the T_2 pressure in the helium coolant so that the tritium permeation in the steam generator (SG) is not excessive. The tritium partial pressure is reduced, therefore, by the addition of oxygen into the helium so that T_2O is formed. While the uncatalyzed reaction rate for the oxidation of hydrogen is low, recent experimental studies[1] indicate that when tritium permeates through a steel tube which is externally coated with an oxidized surface greater than 95% of the tritium is in the oxidized form. For this study we assume that 99% of the tritium can be oxidized with careful oxidation of the steel. Additionally, investigators[2] conclude that an oxidized steel surface retards the permeation of hydrogen as compared to an unoxidized surface. This retardation effect increases as the

hydrogen partial pressure decreases. Based upon these models, we have prepared Fig. III.3-1 for an oxidized surface on ferritic steel which indicates that the permeation rate for T_2 is decreased by a factor of $\sim 10^2$ at 10^3 Pa(T_2) which is the typical T_2 pressure in the liquid breeder alloy. At the T_2 partial pressure in the helium typical of that found in the SG, the permeation rate decreases by $> 10^3$ times as compared to the unoxidized surface in which the permeation rate is a function of the square-root of the hydrogen pressure. These retardation effects were utilized in this study.

For the blanket selected, all of the bred tritium generated in the liquid alloy breeder must be removed either by permeation through the coolant tubes into the helium or by permeation through the cell walls directly into the plasma chamber where it will be processed with the plasma-exhaust gases. Based upon the dimensions of the blanket and the respective barrier factors for tritium permeation, it is calculated that nearly 72% (8.5×10^{-4} moles T_2/s) permeates into the plasma chamber while 28% (3.3×10^{-4} moles T_2/s) permeates into the helium coolant. Of the tritium in the helium only 3.3×10^{-6} moles/s exists in elemental form, T_2, which can permeate at the SG.

In order to assess the potential for tritium permeation at the SG, the following calculation was made: a side-stream of the fraction, $\dot{\nu}$, of the total helium flow was diverted for $T_2O + T_2$ removal, resulting in a steady-state concentration of the tritium in the helium. The permeation rates of T_2 through the SC were then calculated for this range of T_2 concentrations. The results of Fig. III.3-2 show that the tritium release rate decreases rapidly from 54 Ci/d at $\dot{\nu}$ = 0.5% to 21 Ci/d at $\dot{\nu}$ = 3% and then decreases more slowly as $\dot{\nu}$ increases. The guidelines for the release of tritium from a fusion power plant have not been determined; therefore, we cannot determine the appropriate

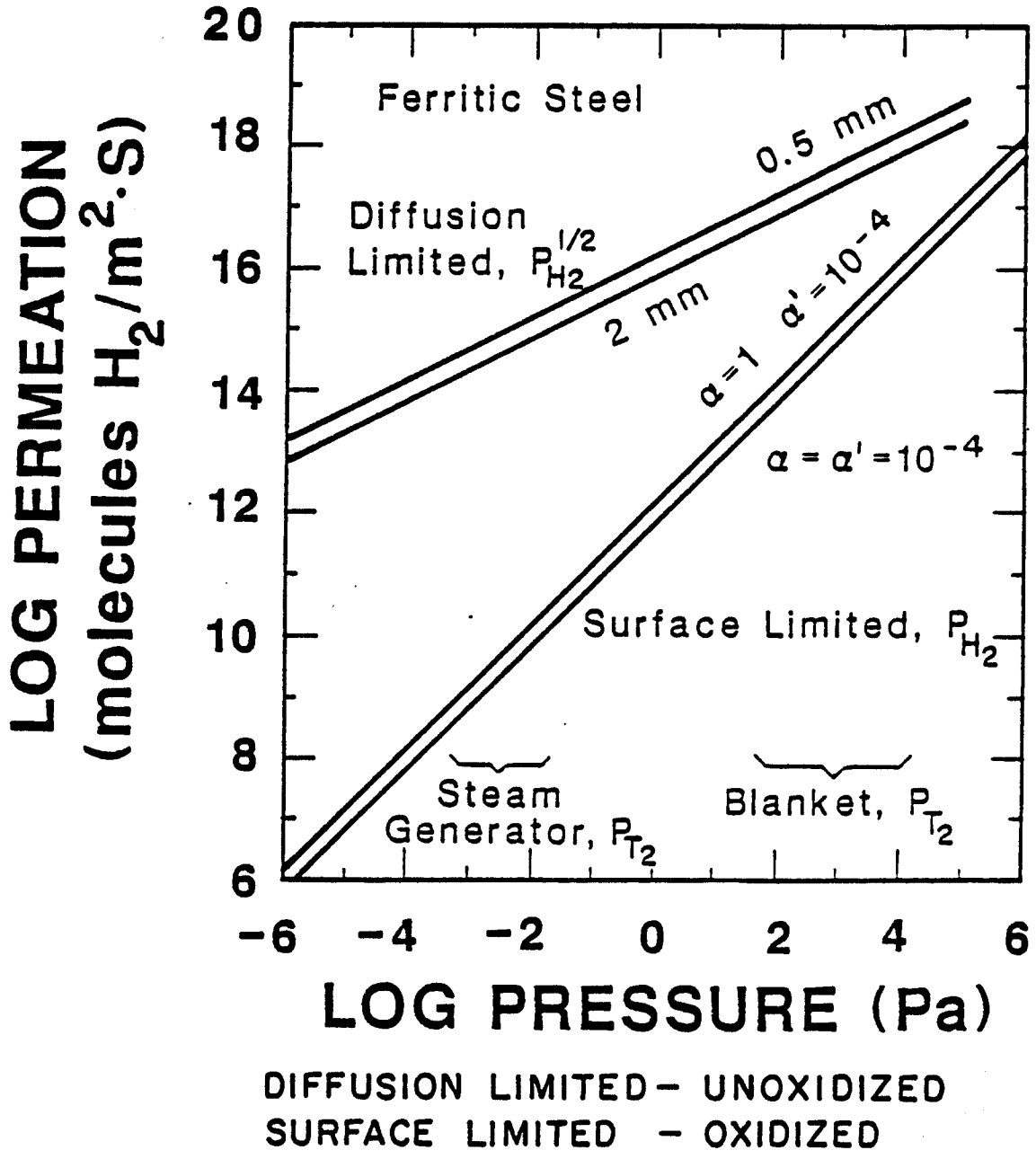

Fig. III.3-1. H_2 permeation through ferritic steel as a function of pressure.

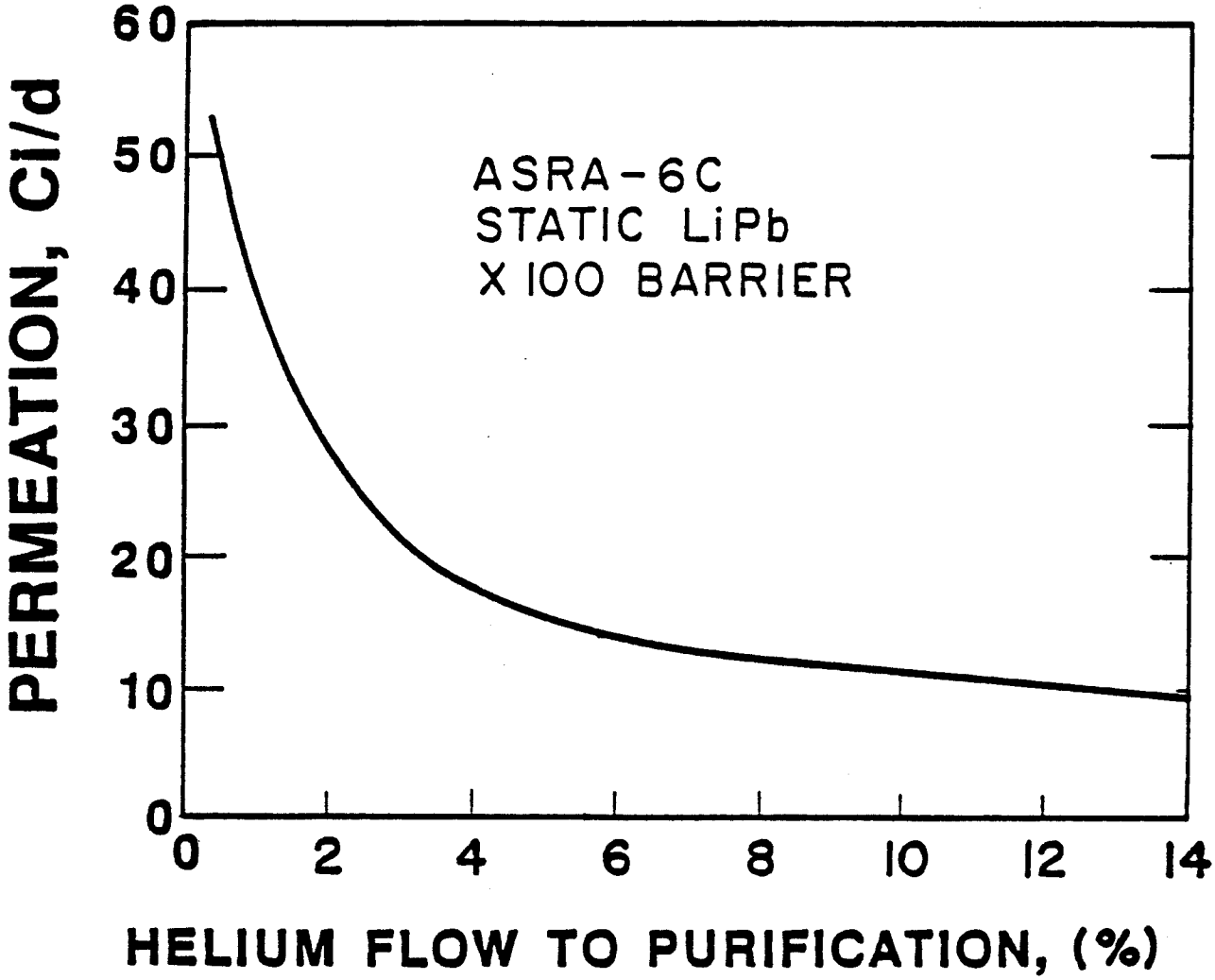

Fig. III.3-2. T_2 permeation into steam generator as a function of the helium purification rate.

value for $\dot{\nu}$ at this time. As a guide to this limit, a recent study[3] has shown that the radiation dose to an individual living 1 km from a chronic emission of tritiated water vapor at the rate of 100 Ci/d is in the range of 5-10 mrem/yr which is within the U.S. Environmental Protection Agency limit; therefore, a modest helium purification rate, 0.5%, appears to be adequate for the initial ASRA-6C design. The inventory of T_2O in the helium coolant is 6.8 g(T). If the helium circuit is constructed to the same high standards as the Dragon Reactor,[4] then the tritium leakage from the circuit should be only 34 Ci/d.

The inventory of tritium within the liquid metal breeder is an important consideration but more difficult to quantify because of conflicting experimental data. Based upon the steady-state tritium permeation rate from the blanket modules, the partial pressure of T_2 within each module is calculated to be 5.1 kPa (T_2). The concentration of tritium in the liquid alloy at this T_2 pressure is determined by use of the Sievert's constant; however, two ranges of experimental values for K_S have been reported:[5,6,7,8] 4.6×10^5 and 5.0×10^4 $kPa^{1/2}$/mole fraction T per mole of $Li_{17}Pb_{83}$. Calculations based upon these two values for K_S indicate the tritium inventory in the entire liquid alloy could be either 49 or 445 g.

The above values are predicted for a well-stirred solution in which the tritium is homogeneously distributed throughout the liquid; however, for this proposed blanket the liquid alloy fills only 14% of the volume around the Be spheres. As a result the liquid will not circulate and tritium can migrate to the walls only by the diffusional process. In this case, the inventory of tritium is given by the relationship,

$$C_T = \frac{\dot{T}\, r^2}{4D} + C_o,$$

where, $\dot{T}$ = the tritium generation rate

r = the radius of the blanket module

D = the diffusion coefficient for T in LiPb (5×10^{-4} cm^2/s)

and C_o = the gaseous solubility of T_2 in the liquid alloy.

The first-term on the right-hand side of the above equation amounts to an additional 287 g(T). When combined with the previously determined values from C_o, the total tritium inventory in the blanket would be 336 or 732 g(T), giving mole fraction tritium concentrations of 33 and 73 appm, respectively. The tritium concentration in this alloy is important because the solubility limit has been reported to be near 10 appm by Wu,[7] 77 appm by Pierini[6] and > 400 appm by Katsuta.[8] Based upon the latter two values, it appears that the solubility limit for tritium in this alloy is not exceeded. If the solubility limit is exceeded, the diffusion of tritium through solid LiT would be approximately five-fold slower; thus, increasing the tritium inventory.

During the second phase of this study, an alternative scheme for the removal of tritium from the breeder alloy will be considered in which the liquid breeder is circulated outside of the reactor for tritium removal, but not for heat removal.

References

1. D.F. Holland and G.R. Longhurst, "Modelling and Experiments on Tritium Permeation in Fusion Reactor Blankets," Fusion Tech., 8, 2067 (1985).

2. M.A. Pick and K. Sonnenbeg, "A Model for Atomic Hydrogen-Metal Interactions-Applications to Recycling, Recombination and Permeation," J. Nuclear Materials, 131, 208 (1985).

3. R. Stasko, "Memo on MINIMARS Radiological Safety," Canadian Fusion Fuels Technology Project, Ontario, Canada (July 1985).

4. B.G. Chapman, "Dragon Operating Experience," in Proc. Gas-Cooled Reactor Information Mtg., Oak Ridge, TN, April 27-30, 1970, CONF-700401 (1970).

5. Y.C. Chan and E. Veleckis, "A Thermodynamic Investigation of Dilute Solutions in the Liquid Li-Pb Alloys," J. Nuclear Materials, 122 & 123, 935 (1984).

6. G. Kuhlborsch and R. Reiter, "Physical Properties and Chemical Reaction Behavior of $Li_{17}Pb_{83}$ Related to Its Use as a Fusion Reactor Blanket," Nuclear Eng. Design/Fusions, 1, 195 (1984).

7. C.H. Wu, "The Interaction of Hydrogen Isotopes with the Li-Pb Alloys," J. Nuclear Materials, 122 & 123, 941 (1984).

8. H. Katsuta, H. Iwamoto and H. Ohno, "Hydrogen Solubility in Liquid $Li_{17}Pb_{83}$," J. Nuclear Materials, 133 & 134, 167 (1985).

IV. MAGNET SHIELDING

IV.1 Magnet Radiation Limits

The magnet radiation limits determine the required shield thickness and magnet size which directly influence the cost of electricity. The superconducting magnet components most sensitive to radiation are the superconductor, the stabilizer, and the insulators. The radiation effects are related since they are determined by the flux level at the magnet. A rule of thumb that holds within a factor of ~ 2 is that a peak winding pack power density of 0.1 mW/cm^3 corresponds to 2 x 10^{18} n/cm^2 (E_n > 0.1 MeV) end of life fluence, 2 x 10^9 rads end of life dose in the insulators, and 10^{-4} dpa/FPY in the Cu-stabilizer.

The critical properties of Nb_3Sn are sensitive to nuclear radiation because of the long range ordered atomic structure. Figure IV.1-1 shows the variation of T_c and J_c for Nb_3Sn with fast neutron fluence (E_n > 0.1 MeV) after 400 K irradiation.[1] The critical current density J_c drops to its preirradiation value at ~ 10^{19} n/cm^2. The initial rise in J_c increases for larger fields and lower irradiation temperatures. Cryogenic temperature irradiation in RTNS-II[2] resulted in a factor of 3 increase in J_c at a fluence of ~ 10^{19} n/cm^2 (E_n > 0.1 MeV). In this study we use an optimistic fluence of 4 x 10^{19} n/cm^2 allowing for proper optimization of Nb_3Sn for nuclear applications. Figure IV.1-1 indicates that T_c drops by ~ 30% at this fluence.

Mechanical strength tests have shown that polyimides are 5 to 10 times more radiation resistant than epoxies.[3] Following irradiation by ~ 10^{10} rads of gamma rays at 5 K, glass fiber filled (gff) polyimides retained 65% of their flexural and compression strength. Recently, 0.5 mm thick disks of gff polyimide were irradiated at 325 K to a mixed gamma and neutron dose of

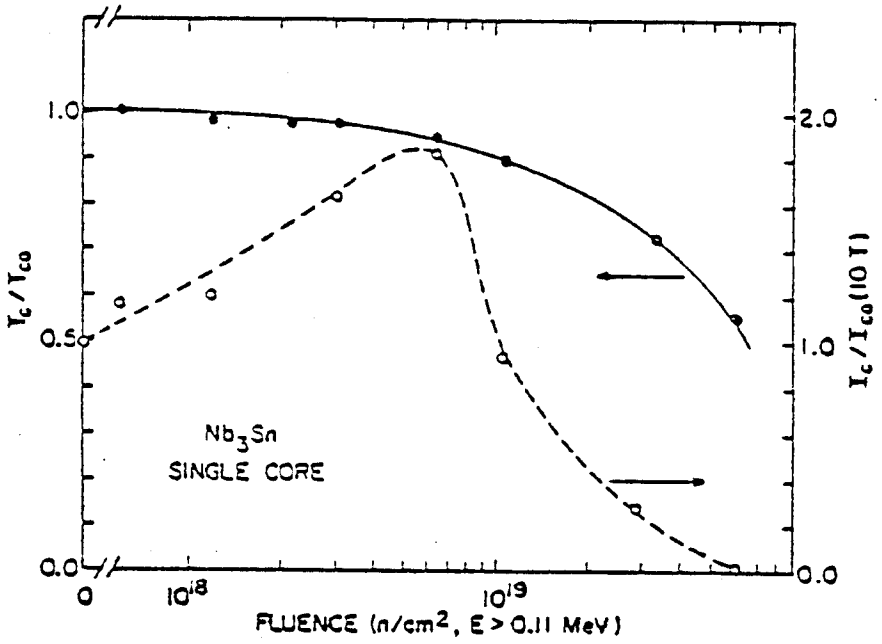

Figure IV.1-1. Fluence effect on T_c and J_c for Nb_3Sn.

$\sim 1.2 \times 10^{12}$ rad with no failures observed in the static compression tests with 2750 MPa stress level.[4] Such a limit can be used if the insulator is designed to be loaded in compression only with no interlaminar shear. However, this dose corresponds to an excessive neutron fluence of $\sim 10^{21}$ n/cm^2. We use a dose limit of 5×10^{10} rads that corresponds to the fluence limit for Nb_3Sn. This dose limit allows for possible insulator material improvement. The superinsulator is exposed to doses higher than those in the electrical insulator. Aluminized kapton can stand doses of $\sim 10^{10}$ rad. Aluminum sheets supported with glass paper that are more radiation resistant will be used for superinsulation in ASRA-6C.

Neutron irradiation at cryogenic temperatures produces defects in the stabilizer resulting in radiation induced resistivity. If we adopt the conservative principle of cryogenic stabilization, the Cu dpa rate is limited to $\sim 5 \times 10^{-5}$ dpa/FPY. This is a very restrictive limit and corresponds to end of life fluence of only $\sim 10^{18}$ n/cm^2. Options for relaxing this limit include using a cable in conduit design as in the ASRA-6C magnets. Hence, we do not set a limit on damage to the Cu stabilizer in ASRA-6C.

Although winding pack power densities as high as ~ 1 W/cm^3 can be handled by the liquid helium coolant, the values that can be achieved in practice are much lower because of problems of cryogen replenishment for the He-I cooled ASRA-6C magnets. The optimum nuclear heating level can be determined from a cost tradeoff analysis, where the total cost of the shield, magnet, and cryoplant is minimized. Optimization calculations have been performed for the central cell and choke coil magnets of MINIMARS.[5] The optimum peak winding pack power densities were found to be 0.04 and 0.25 mW/cm^3, respectively. The cost minima are quite broad. A limit of 0.1 mW/cm^3 on the poloidal average of

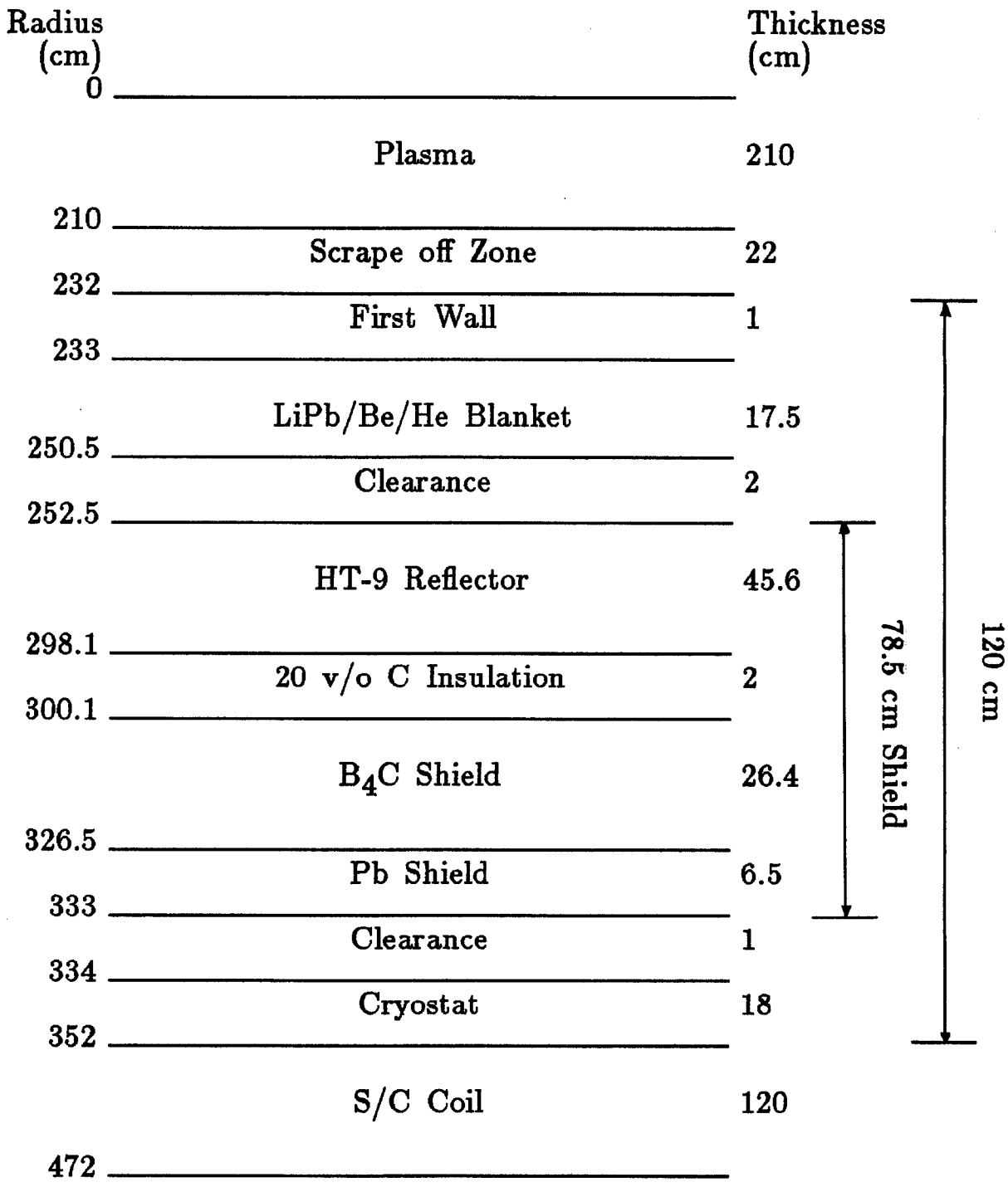

Figure IV.2-1. Radial build of the blanket, shield, and magnet used in the neutronics calculations for ASRA-6C.

the peak winding pack power density is used in ASRA-6C. This was determined also by requiring that no more than a few percent of the gross electric power be recirculated for the cryoplant. Although this limit is quite small and corresponds to nominal (poloidal average) peak fluences and doses of only $\sim 2 \times 10^{18}$ n/cm^2 and $\sim 2 \times 10^9$ rad, the higher dose and fluence limits used in this study are needed to allow for magnet hot spots as long as the higher nuclear heating at these hot spots does not significantly increase the total cryogenic load. The 0.1 mW/cm^3 limit was the reason for designing the ASRA-6C coils with a 1.2 m space between the first wall and the magnet winding pack.

IV.2 Shield Neutronics

Considering the optimistic magnet radiation limit adopted in this study, we find that the magnet shield is driven by the nuclear heating in the magnet. Hence, the optimum shield composition is determined such that the peak winding pack power density is minimized. We performed a study to optimize the shield behind the thin LiPb/Be/He blanket using the ONEDANT code.[6] We selected the option of alternate materials with a thick layer of Fe-shield followed by a layer of B_4C-shield and then a layer of Pb-shield. The 3 layers were varied in thickness to reduce the peak nuclear heating in the magnet. The optimum shield was found to consist of 58.1% Fe-shield (acts also as the reflector), 33.6% B_4C-shield, and 8.3% Pb-shield. While the Fe-shield is run hot and cooled by the He gas used to cool the blanket, the B_4C and Pb-shields are water cooled. Figure IV.2-1 gives a schematic of the blanket, shield and superconducting magnet in ASRA-6C. The plasma and first wall dimensions at the reactor midplane were used in the calculations, since the results of Section III.2 indicate that the peak wall loading and magnet hot spots occur at the midplane. The material composition used for the different zones in the calculations is given in Table IV.2-1.

Table IV.2-1. Material Composition for the Different Zones

First Wall	50 v/o HT-9
	50 v/o He
Blanket	14 v/o LiPb
	53 v/o Be (90% d.f.)
	11 v/o HT-9
	22 v/o He/void
Reflector	90 v/o HT-9
	10 v/o He
B_4C Shield	80 v/o B_4C (87% d.f.)
	10 v/o HT-9
	10 v/o H_2O
Pb Shield	80 v/o Pb
	10 v/o HT-9
	10 v/o H_2O
Cryostat	1 cm Vacuum Vessel (304 SS)
	5 cm Thermal Insulation (5 v/o Kapton)
	1 cm LN_2 Radiation Shield
	10 cm Coil Case (95 v/o 304 SS, 5 v/o LHe)
	1 cm GFF Polyimide (45 v/o poly., 55 v/o S-glass)
S/C Coil	20 v/o 304 SS
	40 v/o Cu
	12 v/o Nb_3Sn
	18 v/o He
	10 v/o GFF Polyimide

The peak radiation effects in the magnet were calculated by normalizing the results to a neutron wall loading of 2.4 MW/m^2. This is the peak wall loading that occurs on the outboard side of the midplane at the five toroidal locations where the plasma is horizontal as indicated by the results of Section III.2. These peak radiation effects are given in Table IV.2-2. The peak values for neutron fluence and dose to the electrical insulator are well below the specified limits. They are even lower than the commonly used conservative limits (4×10^{18} n/cm^2 and 10^{10} rad). The dpa rate in Cu corresponds to 27 $n\Omega$ cm radiation induced resistivity after 4 FPY when the first annealing is needed. However, as indicated in Section IV.1, cryogenic stability is not a concern here since a cable in conduit design is used. Also, the dose to the superinsulator is not of concern as glass reinforced aluminum sheets are used.

Using the neutron wall loading distribution given in Section III.2 we calculated the average nuclear heating at the inner bore of the magnet to be 0.06 mW/cm^3. The He-coolant manifolds result in local hot spots with damage of about a factor of 5 higher than the nominal value. This results in peak fluence and dose values of $\sim 10^{19}$ n/cm^2 and $\sim 10^{10}$ rad. These are well below the optimistic limits and slightly higher than the conservative limits. The peak values can be reduced further by properly placing the headers at poloidal locations with lower wall loading. Since the headers occupy a small fraction ($\sim$ 15%) of the blanket poloidal length, the average heating at the inner bore will increase by a factor of $\sim$ 1.6 to 0.096 mW/cm^3 which remains below the 0.1 mW/cm^3 limit. The nuclear heating per cm toroidal length of the magnet was calculated to be 2.35 and 4.21 W/cm for the winding pack and coil case, respectively. Since 30 coils each with an axial width of 1 m are used in

Table IV.2-2. Peak Radiation Effects in Magnets

Winding pack power density, mW/cm^3	0.103
Fast neutron fluence (E_n > 0.1 MeV), n/cm^2 @ 20 FPY	2.2×10^{18}
DPA rate in Cu stabilizer, dpa/FPY	9.5×10^{-5}
Dose in gff polyimide electrical insulator, rad @ 20 FPY	1.95×10^{9}
Dose in Superinsulator, rad @ 20 FPY	1.11×10^{10}

ASRA-6C, the total nuclear heat in the magnets is 19.7 kW. These results indicate that ~ 0.4% of the electric power has to be recirculated to remove the nuclear heating from the magnets.

References

1. C. Snead, Jr. et al., J. Nucl. Mat., 103 & 104, 749 (1981).

2. M. Guinan, et al., "RTNS-II 1983 Annual Report," UCID-19837-83, Lawrence Livermore National Lab. (1983).

3. R. Coltman and C. Klabunde, J. Nucl. Mat., 103 & 104, 717 (1981).

4. R. Schmunk, EG&G Idaho, Inc., Private Communication, March 1985.

5. B. Logan, et al., "MINIMARS Interim Report," to be published, Lawrence Livermore National Lab. (1985).

6. R. O'Dell et al., "User's Manual for ONEDANT: A Code Package for One-Dimensional, Diffusion-Accelerated, Neutral Particle Transport," LA-9184-M, Los Alamos National Laboratory (1982).

V. MAGNET WINDING CONSIDERATIONS

V.1 Introduction

Prediction of the detailed shape taken by twisted windings, such as those in modular stellarators, requires use of differential geometry. In the present work, the mathematical tools required for such a description are developed.

Two different approaches to the problem of defining twisted coil windings can be used. The first is to start with a defining surface (e.g. a toroid for modular stellarators) and define a closed curve on the defining surface in terms of a relation between two surface parameters. The second approach is to start with a space curve, which may be defined by the defining surface, or by some other method, and construct a particular winding surface, called the rectifying developable, from it. The rectifying developable offers distinct advantages in coil fabrication, including the fact that the turns in a layer are geodesics on it.

In the present work, it is assumed that turns have constant transverse dimensions and that effects due to deformation of individual turns can be neglected; the latter approximation is good for coils with many turns and conversely for those with few turns.

V.2 Description of Work

Given a surface with cartesian coordinates $\vec{R}(p,q)$, where p and q are surface parameters, and a starting curve representing the first or central turn in a layer, the problem is to find the family of curves on $\vec{R}$ parallel to the starting curve, that is, the loci of points which are a constant arc length away from the starting curve along the geodesics orthogonal to the starting curve. Finding the positions of successive turns in a layer

therefore reduces to the problem of finding the family of geodesics orthogonal to an arbitrary curve on a surface. General solution of the above problem requires solution of the geodesic equations:[1,2]

$$\frac{d^2p}{ds^2} + \Gamma_1^{11}\left(\frac{dp}{ds}\right)^2 + 2\Gamma_1^{12}\frac{dp}{ds}\frac{dq}{ds} + \Gamma_1^{22}\left(\frac{dq}{ds}\right)^2 = 0 \tag{1}$$

$$\frac{d^2q}{ds^2} + \Gamma_2^{11}\left(\frac{dp}{ds}\right)^2 + 2\Gamma_2^{12}\frac{dp}{ds}\frac{dq}{ds} + \Gamma_2^{22}\left(\frac{dq}{ds}\right)^2 = 0 \tag{2}$$

where the Γ_k^{ij} are Christoffel symbols and contain first and second derivatives of the vector function $\vec{R}(p,q)$. From the theory of differential equations, it is known that the above equations have a unique solution when the initial values p and q and derivatives dp/ds and dq/ds are specified along the starting curve. Values for the derivatives along the curve are in turn readily determined from the defining relation for the curve.

As successive layers are wound on a coil, the surfaces so formed constitute a family of parallel surfaces, described by the following parametric form

$$\vec{R}^*(p,q,h) = \vec{R}(p,q) + h\hat{N}(p,q) \tag{3}$$

where h is the winding depth, fixed for a particular layer. Parallel turns are found as before by constructing the family of geodesics parallel to the starting curve, which must be specified independently for each layer. Explicit expressions for the Christoffel symbols of the parallel surface in terms of the first, second, and third derivatives of the starting surface $\vec{R}$ have been derived in present work. Also, possible prescriptions for specifying the new starting curve for each layer are discussed.

Various authors[3,4] have discussed the advantages of using the rectifying developable as a winding surface; among the advantages are the lack of the need for continuous clamping in winding, ease of fabrication of the coil bobbin, and the fact that flat (low height-to-width ratio) conductors can be used due to the lack of bends around both conductor faces. The rectifying developable, as derived from a space curve $\vec{r}_o(s_o)$, has the following parametric form:

$$\vec{R}(s_o,l) = \vec{r}_o(s_o) + l\hat{p}(s_o) \tag{4}$$

where the unit vector $\hat{p}$ is given by the expression

$$\hat{p}(s_o) = \frac{\frac{\tau}{\kappa}\hat{t} + \hat{b}}{[1 + (\tau/\kappa)^2]^{1/2}} \quad . \tag{5}$$

In the above τ is the torsion and κ the normal curvature of the space curve. It can be easily shown that $\vec{r}_o(s_o)$, as desired, is a geodesic on the surface; the parallel curves are also geodesics and can be written in the form

$$\vec{r}_o(s_o) = \vec{r}_o(s_o) + u(s_o)\hat{p}(s_o) \tag{6}$$

where $u(s_o)$ is the length between $\vec{r}$ and $\vec{r}_o$ along the vector $\hat{p}(s_o)$. An expression has been derived for $u(s_o)$; writing σ for τ/κ, the result is

$$u(s_o) = u_o\left|\frac{\bar{1} + \sigma^2(s_o)\bar{}}{\bar{1} + \sigma^2(o)\bar{}}\right|^{1/2} = u_o \frac{\sin\phi\ (o)}{\sin\phi\ (s_o)} = \frac{w}{\sin\phi\ (s_o)} \quad . \tag{7}$$

In the above equation, u_o is the value of u at $s_o = 0$, ϕ the angle between $\hat{p}$ and $\vec{r}_o$, and w the constant width between $\vec{r}_o$ and $\vec{r}$ along the geodesics orthogonal to $\vec{r}_o$. The above expression was used to show explicitly that the curves parallel to $\vec{r}_o$ have the same length as $\vec{r}_o$ when $\vec{r}_o$ is a closed curve.

Finally, expressions for the family of surfaces parallel to the rectifying developable and their geodesics were derived; the parallel surface has the form

$$\vec{R}(s_o,l,h) = \vec{r}_o(s_o) - \hat{n}_o(s_o)h + l\hat{p}_o(s_o) \tag{8}$$

where $\hat{n}_o$ is the principal normal to $\vec{r}_o$. Equation (8) also describes a developable surface. If the angle between the geodesics on the parallel surface and $\vec{r}_o$ for a given value of s_o is chosen to be zero, then the family of geodesics on the parallel surface takes the form

$$\vec{r}(s_o,h,w) = \vec{r}_o(s_o) - \hat{n}_o(s_o)h + u(s_o,h,w)p(\hat{s}_o) \tag{9}$$

where $u(s_o,h,w)$ is given by

$$u(s_o,w) = \frac{h}{\sin\phi\ (s_o)} \int_0^{s_o} \tau(s)ds + \frac{w}{\sin\phi\ (s_o)} . \tag{10}$$

The cross section of the resultant winding pack for constant layer width in the $\hat{p}$ - $\hat{n}_o$ plane is a parallelogram with sides inclined from $\hat{n}_o$ by the angle

$$\Psi = \tan^{-1}\left[\frac{1}{\sin\phi} \int_0^{s} \tau_o(s)ds\right] . \tag{11}$$

V.3 Results

The general mathematical framework for describing the detailed shape taken by twisted coil windings as they are wound has been developed, using the techniques of differential geometry. The geometry of a particular winding surface, the rectifying developable, and its parallel surfaces is described. The results are expected to be useful in the detailed design of twisted coils and their winding hardware.

References

1. A.R. Forsyth, Lectures on the Differential Geometry of Curves and Surfaces, Cambridge Univ. Press, 1912.

2. L.R. Eisenhart, A Treatise on the Differential Geometry of Curves and Surfaces, Ginn and Co., Boston, 1909.

3. B. Colyer, "The Geometry of Constant Perimeter Dipole Windings," Rutherford Laboratory Report RL-73-143, Nov. 1973.

4. R.L. Brown, "A New Design Principle for Three-Dimensional Magnet Windings," from Oak Ridge National Laboratory Report ORNL-4545, pp. 155-159, Dec. 1969.

VI. CONCLUSIONS AND RECOMMENDATIONS

The major conclusions from this year's activity are listed below:

A. Even though the magnetic pumped limiter design appears to be promising in terms of particle collection, its sensitivity to small variations in magnetic fields has caused us to put this concept aside for now and pursue an alternate magnetic scheme for impurity control.

B. The use of modest RF powers to promote the removal of impurities still remains promising and it will continue to be investigated.

C. It has been shown that a thin (17.5 cm) blanket of HT-9/PbLi/Be with helium cooling can satisfy the tritium breeding and energy multiplication functions of a commercial power blanket for ASRA-6C.

D. Poloidal and toroidal considerations of the neutron wall loading reveal that the maximum value is 2.4 MW/m^2 and the average wall loading is 1.4 MW/m^2.

E. A blanket design, compatible with 80 atmosphere helium cooling and multiple penetrations for RF or NBI heating, appears to be feasible. Furthermore, this blanket is easily removed for maintenance and presents the possibility of inherent safety even in the event of LOF or LOC accidents.

F. An efficient 78.5 cm shield of HT-9/C/B_4C/Pb has been shown to effectively protect the S/C coils of ASRA-6C. This shield reduces the nuclear heating to ~ 0.1 MW/cm^3 and allows the winding pack of the coil to be placed 120 cm from the first wall.

G. A general mathematical framework for describing the detailed shape taken by twisted coil windings as they are wound has been developed.

This past work suggests critical issue areas which need to be examined in the near future for ASRA-6C. These are listed below:

A. Increased effort is required to develop a magnetic limiter approach compatible with the complex plasma shape in a stellarator.

B. Continued investigations of the RF technique for impurity control is necessary as a backup for magnetic limiters.

C. More detailed thermal and stress analysis of the ASRA-6C blanket is required to validate its projected long term operation.

D. A more detailed radiation damage analysis of the ASRA-6C blanket and S/C magnets is required to validate the thin blanket and shield design proposed during the 1985 study.

E. Safety analyses need to be initiated to demonstrate the promise of ASRA-6C blanket.

F. A closer coupling of the ASRA-6C nuclear island to the balance of plant design and an economic analysis needs to be initiated. In particular, an overall systems costing code is needed to guide the future decisions made with respect to optimum power level and operating temperatures.

In summary, a very solid start on the ASRA-6C power reactor design was made in 1985. With a few more years of this level of effort, a more complete design should be available on the level of the UWMAK, STARFIRE or MARS designs. At that time the advantages of a steady state stellarator design should be more apparent.